# Accepted Manuscript

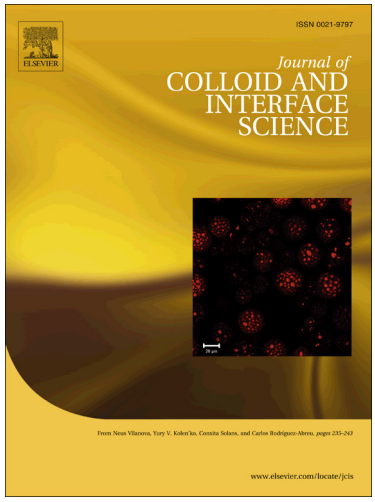


Synthesis and application of a new carboxylated cellulose derivative. Part I: Removal of $Co^{2+}$, $Cu^{2+}$, and $Ni^{2+}$ from monocomponent spiked aqueous solution

Filipe Simões Teodoro, Stela Nhandeyara do Carmo Ramos, Megg Madonyk Cota Elias, Aparecida Barbosa Mageste, Gabriel Max Dias Ferreira, Luis Henrique Mendes da Silva, Laurent Frédéric Gil, Leandro Vinícius Alves Gurgel

PII: S0021-9797(16)30553-7
DOI: http://dx.doi.org/10.1016/j.jcis.2016.08.004
Reference: YJCIS 21472

To appear in: *Journal of Colloid and Interface Science*

Received Date: 2 June 2016
Revised Date: 20 July 2016
Accepted Date: 1 August 2016

Please cite this article as: F.S. Teodoro, S.N.d. Ramos, M.M.C. Elias, A.B. Mageste, G.M.D. Ferreira, L.H.M. Silva, L.F. Gil, L.V.A. Gurgel, Synthesis and application of a new carboxylated cellulose derivative. Part I: Removal of $Co^{2+}$, $Cu^{2+}$, and $Ni^{2+}$ from monocomponent spiked aqueous solution, *Journal of Colloid and Interface Science* (2016), doi: http://dx.doi.org/10.1016/j.jcis.2016.08.004

# Synthesis and application of a new carboxylated cellulose derivative. Part I: Removal of $Co^{2+}$, $Cu^{2+}$, and $Ni^{2+}$ from monocomponent spiked aqueous solution

Filipe Simões Teodoro[1], Stela Nhandeyara do Carmo Ramos[1], Megg Madonyk Cota, Elias[1], Aparecida Barbosa Mageste[1], Gabriel Max Dias Ferreira[2], Luis Henrique Mendes da Silva[2], Laurent Frédéric Gil[1], Leandro Vinícius Alves Gurgel[1,*]

[1] Grupo de Físico–Química Orgânica, Departamento de Química, Universidade Federal de Ouro Preto, Campus Universitário Morro do Cruzeiro, s/nº, Bauxita, 35400–000 Ouro Preto, Minas Gerais, Brazil.

[2] Grupo de Química Verde Coloidal e Macromolecular, Departamento de Química, Centro de Ciências Exatas, Universidade Federal de Viçosa, Av. P. H. Rolfs, s/nº, 36570–000 Viçosa, Minas Gerais, Brazil.

*Corresponding author. Tel.: +55 31 3559 1744; fax: +55 31 3559 1707; E–mail addresses: legurgel@iceb.ufop.br / legurgel@yahoo.com.br (L.V.A. Gurgel)

**Abstract**

A new carboxylated cellulose derivative (CTA) was prepared from the esterification of cellulose with 1,2,4–Benzenetricarboxylic anhydride. CTA was characterized by percent weight gain (*pwg*), amount of carboxylic acid groups ($n_{COOH}$), elemental analysis, FTIR, TGA, solid-state $^{13}C$ NMR, X-ray diffraction (DRX), specific surface area, pore size distribution, SEM and EDX. The best CTA synthesis condition yielded a *pwg* and $n_{COOH}$ of 94.5% and 6.81 mmol.g$^{-1}$, respectively. CTA was used as an adsorbent material to remove $Co^{2+}$, $Cu^{2+}$ and $Ni^{2+}$ from monocomponent spiked aqueous solution. Adsorption studies were developed as a function of the solution pH, contact time and initial adsorbate concentration. Langmuir model better fitted the experimental adsorption data and the maximum adsorption capacities estimated by this model were

0.749, 1.487, and 1.001 mmol.g$^{-1}$ for $Co^{2+}$, $Cu^{2+}$ and $Ni^{2+}$, respectively. The adsorption mechanism was investigated by using isothermal titration calorimetry. The values of $\Delta_{ads}H°$ were in the range from 5.36 to 8.09 kJ.mol$^{-1}$, suggesting that the mechanism controlling the phenomenon is physisorption. Desorption and re–adsorption studies were also performed. Desorption and re–adsorption efficiencies were closer to 100%, allowing the recovery of both metal ions and CTA adsorbent.

**Keywords:** Carboxylated cellulose; 1,2,4–Benzenetricarboxylic anhydride; adsorption; desorption; isothermal titration calorimetry; thermodynamics.

## 1. Introduction

Contamination of water resources by toxic heavy metals via the discharge of untreated or partially treated industrial wastewaters is considered as a serious worldwide environmental problem [1-3]. The release of toxic heavy metals to water streams has seriously increased due to rapid industrialization mainly in developing countries. Industrial activities such as mining operations, electronics, electroplating, metal processing, textile, battery manufacturing, tanneries, pesticides, petroleum refining, paint manufacture, pesticides, pigment manufacture, printing and photographic are considered as the major sources of contamination by heavy metals in the ionic form [1, 4-6].

The Agency for Toxic Substances and Disease Registry (ATSDR) [7] has classified some metals as toxic, persistent and bioaccumulative [5]. Metals such as arsenic (As), cadmium (Cd), chromium (Cr), cobalt (Co), copper (Cu), lead (Pb), mercury (Hg), nickel (Ni) and zinc (Zn) have been recognized as hazardous to health, being that Co, Ni and Cu occupy the positions 51, 57, and 118 in the list of most harmful metals of ATSDR [1, 7, 8]. The toxicity of heavy metals results in serious damage to central

nervous system and blood composition, lungs, kidney, liver and other vital organs [1]. In addition, the contamination of water streams and marine water by toxic heavy metals also causes a serious health hazard to the aquatic living organisms [1, 9]. As a consequence, in many countries, more rigorous legislation has been implemented to regulate water pollution by toxic heavy metals [9]. For example, Ahmaruzzaman [1] lists the most rigorous permissible limits in the world for industrial effluent discharges and drinking water according to World Health Organization (WHO), US Environmental Protection Agency (USEPA), and European Union (EU) as well as some health effects of various toxic heavy metals.

There are various treatment processes available for treating waste streams contaminated with toxic heavy metals such as chemical precipitation, coagulation, solvent extraction, ultrafiltration, biological systems, electrolytic processes, reverse osmosis, oxidation with ozone/hydrogen peroxide, membrane filtration, photocatalytic degradation, ion exchange and adsorption [1, 9]. However, adsorption is considered as one of the most effective processes of advanced wastewater treatment to be employed by industries to decrease the concentration of heavy metals in the effluents as it offers flexibility in design and operation, treats effluents containing both low and high concentrations [10] of pollutants and in the majority of the cases produces high-quality treated effluents [1, 9].

Also according to Ahmaruzzaman [1], three of the most important factors for the economic evaluation of the adsorption process are efficiency, which is often measured as adsorption capacity, local availability of the precursor material and preparation cost of the adsorbent material (cost of transportation, milling, chemicals, electrical energy, system for recovery of the chemicals used, among others). Activated carbons (ACs) produced by carbonizing lignocellulosic waste materials are the most widely used

adsorbents and cost about US$ 20.00 per kg [1]. Although, ACs have exhibited capacity to adsorb metal ions, the low adsorption capacity and specificity for adsorption of various types of heavy metals and limited desorption capacity, which causes problems related with their reutilization and disposal, associated to the cost of ACs limits their utilization in wastewater treatment processes [1].

Over the last few years, a great number of researchers have been investigated lignocellulosic materials as natural absorbents. However, the use of these materials in a raw form has some disadvantages such as low adsorption capacity and releasing organic compounds (extractives such as flavonoids, tannins, waxes, among others), which causes the increase of chemical oxygen demand (COD), biological oxygen demand (BOD) and total organic carbon (TOC), thereby causing secondary pollution in water [10]. Hence, the use of biopolymers such as chitosan, cellulose [6, 11], alginate, among others [12, 13] as renewable and biodegradable materials for adsorption has some advantages as they can be chemically modified with organic ligands available commercially or specifically designed, in an attempt to obtain more selective, effective and resistant (good thermal, mechanical and chemical properties) to adsorb metal ions in aqueous solution [6]. The chemical modifications are based on the chemistry of hydroxyl, amine, carbonyl, carboxyl, among other groups available at surface of cellulose, chitosan and alginate [14]. In addition, cellulose is considered as the most renewable biopolymer in nature [15] and can be isolated from lignocellulosic biomass with different pulp grades and costs such as unbleached (Eucalyptus/Birch, US$ 0.10 per kg), semi–bleached or fully bleached (Eucalyptus/Birch, US$ 0.75 per kg) pulp. Cellulosic pulp is more expensive than lignocellulosic biomass (sugarcane bagasse, US$ 0.018 per kg)[16]; however, the yields of the chemical modifications in terms of weight gain are much higher using cellulose pulp than lignocellulosic biomass, which contains

only 15-55% of cellulose in their composition [10]. Furthermore, the specific surface properties of cellulose derivatives can be better controlled as the chemical modifications are easier to be accomplished in comparison with lignocellulosic biomass.

This study aimed to prepare a new adsorbent material from cellulose to remove $Co^{2+}$, $Cu^{2+}$ and $Ni^{2+}$ from monocomponent spiked aqueous solution and thereby to produce an efficient adsorbent resistant to acidic and basic pH values, with high adsorption capacity for metal ions, easy regeneration and reuse. The new adsorbent (CTA) was synthesized by esterification of hydroxyl groups of cellulose with 1,2,4–Benzenetricarboxylic anhydride, which is a commercial and stable reagent. In the first part of this study, the adsorption of $Co^{2+}$, $Cu^{2+}$ and $Ni^{2+}$ on the CTA adsorbent was assessed as a function of the solution pH, contact time (kinetics) and initial metal ion concentration in monocomponent aqueous solution. A suitable desorption process was performed to evaluate the regeneration and reuse of the CTA adsorbent. The enthalpy involved in the adsorption process was also assessed by isothermal titration calorimetry and the adsorption mechanism was discussed.

## 2. Material and methods

### 2.1. Material

$CoCl_2 \cdot 6H_2O$, $CuSO_4 \cdot 5H_2O$, monochloroacetic acid (99%), $CH_3COONa \cdot 3H_2O$ and isopropanol were purchased from Synth (Brazil). 1,2,4-Benzenetricarboxylic anhydride (Trimellitic anhydride, TA) (97%) (cat no. 552-30-7), Whatman® cellulose chromatography papers (20 × 20 cm) (cat no. WHA3001861) and 3 Å molecular sieve (cat no. 69839) were purchased from Sigma–Aldrich (Brazil). $NiCl_2 \cdot 6H_2O$, glacial acetic acid (99.5%), NaOH, HCl (37% w/w), acetone, *N*,*N*-dimethylacetamide (DMA) and pyridine (Py) were purchased from Vetec (Brazil). Quantitative filter paper (black ribbon, JP–41, cat no. 3509–1, 12.5 cm diameter, ash content of 0.00009 g and

grammage of 80 g.cm$^{-2}$) was purchased from JProlab (Brazil). Py was refluxed in a 2 L round–bottom flask with NaOH pellets for 12 h, distilled and stored in a flat–bottom flasks containing NaOH pellets before use. Molecular sieve was previously activated in an oven at 150°C for 2 h. DMA was stored with molecular sieve (3 Å) before use. All metal ion solutions used in the adsorption studies were buffered. Buffers consisting of 0.05 mol.L$^{-1}$ $CH_2ClCOOH/CH_2ClCOONa$ (pH from 2.0 to 3.5) and 0.05 mol.L$^{-1}$ $CH_3COOH/CH_3COONa$ (pH from 4.0 to 5.5) were prepared in deionized water (Millipore, model Milli–Q®).

### 2.2. Esterification of cellulose with trimellitic anhydride

The esterification of cellulose (C) with trimellitic anhydride (TA) to obtain cellulose trimellitate (CTA) was investigated and optimized by studying the effect of TA amount and reaction time on percent weight gain (*pwg*) [Eq. (1)] and amount of carboxylic acid groups released ($n_{COOH}$) [Eq. (2)].

#### 2.2.1. Esterification of C as a function of the amount of TA

Different amounts of TA 2.37, 4.74, 7.11 and 9.48 g corresponding to molar ratios of TA–to–AGU of 2, 4, 6 and 8 were used to investigate the effect of TA on *pwg* and $n_{COOH}$. A typical reaction and elaboration procedure is described as follows: C (pieces of 2 × 2 mm) (1.0 g; 162.14 g.mol$^{-1}$; 6.17 mmol), TA (2.37 g; 192.13 g.mol$^{-1}$; 12.34 mmol), anhydrous DMA (10 mL) and anhydrous Py (10 mL) were added to a round-bottom flask to give a solid–to–liquid ratio of 1:20 (w/v) (C:DMA/Py). The flask was equipped with a reflux condenser attached to a drying tube packed with anhydrous calcium chloride (powder). Then, the flask was put in an oil bath at 100°C placed on a heating plate (Corning®, model PC–420D) and magnetically stirred at 300 rpm for 1 h. At the end of reaction time, the flask was removed from the bath and left to cool (30

min) and the suspension was poured into a 250 mL Becker containing 125 mL of isopropanol [17]. The suspension was magnetically stirred for 30 min before being transferred to a sintered Büchner glass funnel (150 mL; porosity 3). This procedure was repeated twice. Then, CTA was washed in a row with distilled water (100 mL), 0.01 mol.L$^{-1}$ HCl (100 mL), distilled water (100 mL) and isopropanol (50 mL). The white solid (CTA) was dried in an oven at 95°C for 2.5 h, put in a desiccator to cool and weighed until to obtain a constant weight.

### 2.2.2. Esterification of C as a function of reaction time

The amounts of TA of 4.74 and 9.48 g corresponding to molar ratios of TA–to–AGU of 4 and 8 were chosen for the continuation of the studies of esterification of C with TA as a function of reaction time. The reaction times studied were 0.5, 1 and 3 h and 0.5, 0.75, 1, 2 and 3 h for TA–to–AGU molar ratios of 4 and 8, respectively. The other procedures were the same described in Section 2.2.1.

## 2.3. Characterization of CTA

### 2.3.1. Percent weight gain (*pwg*)

The *pwg* after esterification of C with TA was calculated using Eq. (1) as follows:

$$pwg\ /\ \% = \left( \frac{w_{CTA} - w_C}{w_C} \right) \times 100 \quad (1)$$

where $w_{CTA}$ and $w_C$ (g) are the weights of CTA and C.

### 2.3.2. Amount of carboxylic acid groups ($n_{COOH}$)

The $n_{COOH}$ of the CTA was determined by acid–base back titration. Two 0.0800 g samples of the CTA were weighed into 250 mL Erlenmeyer flasks and 100.0 mL of standardized aqueous NaOH solution (10 mmol.L$^{-1}$) was added to each flask. The flasks

were mechanically stirred at 25°C for 60 min at 100 rpm. Then, the suspensions were filtered off using a single filtration (JP–41 filter paper). Three 20.0 mL aliquots from each Erlenmeyer flask were titrated with standardized aqueous HCl solution (10 mmol.$L^{-1}$) until phenolphthalein endpoint. The $n_{COOH}$ of the CTA was calculated using Eq. (2) as follows [5]:

$$n_{COOH} / (\text{mmol/g}) = \frac{\left[C_{NaOH}V_{NaOH} - f\left(C_{HCl}V_{HCl}\right)\right]}{w_{CTA}} \quad (2)$$

where $C_{NaOH}$ and $C_{HCl}$ (mmol.$L^{-1}$) are the concentrations of standardized aqueous NaOH and HCl solutions, respectively, $V_{NaOH}$ (L) is the volume of standardized NaOH solution, $V_{HCl}$ (L) is the volume of standardized HCl solution consumed titrating the excess of unreacted NaOH, $w_{CTA}$ (g) is the weight of the CTA and $f$ is a conversion factor.

### 2.3.3. Determination of point of zero charge (PZC)

The PZC of the CTA was determined using mass titration method developed by Noh and Schwarz [18] with minor modifications. Three solutions of 0.01 mol.$L^{-1}$ $NaNO_3$ (background electrolyte) of initial pH values of 3, 6 and 11 were prepared using aqueous 0.01 mol.$L^{-1}$ $HNO_3$ and aqueous 0.01 mol.$L^{-1}$ NaOH solution to adjust the solution pH. Different amounts of CTA samples were weighed into five 125 mL Erlenmeyer flasks and 20.0 mL of 0.01 mol.$L^{-1}$ $NaNO_3$ solution of pH 3, 6 or 11 was added to each flask to give suspensions of 0.5, 1, 5, 10 and 20% (w/v). The fifteen flasks were mechanically stirred at 25°C for 24 h at 130 rpm (Nova Ética, model 109/2). The equilibrium pH was measured using a pH meter (Hanna Instruments, model HI 223). The PZC was calculated at the convergence point of the three curves.

### 2.3.4. Elemental analysis

The contents of carbon (C), hydrogen (H) and nitrogen (N) in C and CTA were determined by elemental analysis on a Perkin Elmer Series II CHN 2400 analyzer (Shelton, USA).

### 2.3.5. Fourier Transform infrared (FTIR) spectroscopy

Samples of 1.0 mg of C, CTA, CTA–loaded with $Co^{2+}$, $Cu^{2+}$ and $Ni^{2+}$ and CTA after desorption of $Co^{2+}$, $Cu^{2+}$ and $Ni^{2+}$ were mixed to 100.0 mg of spectroscopy grade KBr and pressed in a hydraulic press at 8 tons for 0.5 min to prepare 13 mm KBr pellets (Pike CrushIR, model 181–1110, Pike Technologies, Canada). The FTIR spectra were recorded on an ABB Bomen MB 3000 FTIR spectrometer (Quebec, Canada) equipped with ZnSe optics and a deuterated triglycine sulfate (DTGS) detector set at a resolution of 4 $cm^{-1}$ from 500 to 4000 $cm^{-1}$ and 32 scans per sample.

### 2.3.6. Thermogravimetric analysis (TGA)

The thermograms of C and CTA were recorded on a thermogravimetric analyzer (Mettler Toledo, model TGA/DSC STARe system version 11.00). Samples of C and CTA (5–6 mg), previously dried in an oven at 90°C for 1 h, were weighed in alumina crucibles and analyzed from 25 to 800°C at a heating rate of 20°C.$min^{-1}$ under $N_2$ atmosphere of 100 mL.$min^{-1}$.

### 2.3.7. X–ray diffraction (DRX)

The diffractogram of C and CTA were obtained on a LabX XRD–6100 X–ray diffractometer (Shimadzu) equipped with CuKα radiation ($\lambda$ = 1.5406 Å) and operating at a voltage of 40 kV and a current of 30 mA. The diffractograms were obtained within the 2θ (Bragg angle) range from 4 to 70° at a scan rate of 4°.$min^{-1}$.

The degree of crystallinity of C and CTA was determined using Eq. (3) as follows [19]:

$$X_c = \left( \frac{A_{Cr}}{A_{Cr} + A_{Am}} \right) \times 100 \quad (3)$$

where $A_{Cr}$ and $A_{Am}$ are the integrated Gaussian areas of the crystalline and amorphous phases, respectively.

### 2.3.8. Solid state carbon–13 nuclear magnetic resonance ($^{13}$C SS–NMR)

High resolution Solid–State NMR (SS NMR) spectra of C and CTA were recorded in a Varian INOVA spectrometer operating at $^{13}$C and $^{1}$H frequencies of 88.02 and 350.50 MHz, respectively. A Varian 7–mm Magic Angle Spinning (MAS) double–resonance probe head was used at spinning frequency of 4.5 kHz controlled by a Varian pneumatic system that ensures a rotation stability of ± 2 Hz. Typical π/2 pulse lengths of 5.0 μs were applied to both $^{13}$C and $^{1}$H. To achieve dead–time–free detection all spectra were recorded with a Hahn spin echo generated by an 180° pulse applied one rotation period (tr) after the end of excitation. Time proportional phase modulated (TPPM) proton decoupling with field strength of 60 kHz was used in all experiments. The ramp for Cross–Polarization (CP) was implemented with amplitude increment from 90 to 100%. 13C Multiple CP under MAS (MultiCP) experiments were achieved using nine periods of cross–polarization with time of 1 ms spaced by the repolarization period tz equal to 0.9 s unless for a last CP period of 0.8 ms. The recycle delays were 2 s. MultiCP is a recently proposed method that can provide quantitative 13C nuclear magnetic resonance spectra (NMR) with higher signal–to–noise ratios in a short period of time compared with the standard quantitative direct–polarization NMR. More details on the method along with the pulse sequence can be found in the study of Johnson and Schmidt-Rohr [20].

### 2.3.9. Scanning electron microscopy (SEM)

The surfaces of C and CTA adsorbent were examined on a scanning electron microscope (Tescan/Oxford Instruments, model Vega3 SB), operating at a tungsten filament voltage from 15 to 20 keV and a secondary electron (SE) detector. Samples of C and CTA were previously dried in an oven at 90°C for 1 h and left to cool in a desiccator. Then, samples were fixed on sample holders containing a graphite ribbon and subsequently sputter–coated with gold in a modular high–vacuum coating (Quorum Technologies, model Q150R ES).

### 2.3.10. Energy dispersive X–ray (EDX) spectroscopy

The surface of CTA–loaded with $Co^{2+}$, $Cu^{2+}$ and $Ni^{2+}$ was analyzed on a Vega3 SB SEM–EDX spectrometer (Tescan/Oxford Instruments) operating with a tungsten filament at a voltage of 20 keV and backscattered electron (BSE) detector. Samples of 100 mg of CTA–loaded with metal ions were pressed in a hydraulic press at 8 tons for 1 min to obtain 13 mm pellets. The pellets were sputter–coated with carbon in a Q150R ES modular high–vacuum coating (Quorum Technologies).

### 2.3.11. Specific surface area and pore size distribution

The specific surface area of the CTA adsorbent was measured on a surface area and pore analyzer (Quantachrome, model Nova 1000) using $N_2$ adsorption/desorption isotherms at 77.35 K. CTA sample was degassed at 30°C for 24 h under vacuum at 0.016 mmHg prior to measurement. The amount of $N_2$ adsorbed and desorbed onto CTA was measured on a wide range of relative pressures ($P/P_0$ = 2 ×$10^{-5}$–1.0), where $P$ is the equilibrium pressure and $P_0$ is the saturation pressure [21]. Specific surface area was determined by Brunauer, Emmett and Teller (BET) method [22], while pore size distributions were determined by Barrett, Joyner and Halenda (BJH) method [23].

### 2.3.12. Adsorption experiments

The adsorption experiments of $Co^{2+}$, $Cu^{2+}$ and $Ni^{2+}$ on the CTA adsorbent in monocomponent systems were carried out in batch mode as a function of contact time (kinetics), solution pH and initial metal ion concentration.

#### 2.3.12.1. Adsorption of metal ions on CTA as a function of contact time

Samples of 100.0 mL of each metal–ion solution (0.79 mmol.$L^{-1}$), buffered at pH 5.5 for $Co^{2+}$, $Cu^{2+}$ and $Ni^{2+}$, were added to 250 mL Erlenmeyer flasks and pre–thermostated at 25°C in an orbital shaker incubator for 1 h (Marconi, model MA–830, Piracicaba, SP. Brazil). Afterwards, samples of CTA (20.0 mg) weighed into cylindrical glass bottles (1.8 mm height × 2.2 mm diameter) were transferred to each flak and stirred at 130 rpm for different periods of time. After each period of time, the solids were filtered off by a single filtration (JP–41 filter paper) and the concentration of each metal ion at a time *t* determined by flame atomic absorption spectrophotometer (FAAS) (Hitachi, model Z–8200) at wavelengths of 240.7 nm, 324.8 nm and 232 nm for $Co^{2+}$, $Cu^{2+}$ and $Ni^{2+}$, respectively. The adsorption capacity ($q_t$) of the CTA adsorbent for each metal ion at a time *t* was calculated using Eq. (4) as follows:

$$q_t\ /\left(\text{mmol/g}\right) = \frac{\left(C_i - C_t\right)_{M^{2+}} V_{M^{2+}}}{w_{CTA}} \qquad (4)$$

where $q_t$ (mmol.$g^{-1}$) is the adsorption capacity of a metal ion ($M^{2+}$) on the CTA at a time *t*, $V_{M^{2+}}$ (L) is the volume of metal ion solution, $C_i$ and $C_t$ (mmol.$L^{-1}$) are the metal ion solution concentrations at 0 and time *t*, respectively and $w_{CTA}$ (g) is the weight of the CTA adsorbent.

#### 2.3.12.2. Adsorption of metal ions on CTA as a function of solution pH

Samples of CTA (20.0 mg) were weighed into 250 mL Erlenmeyer flaks, and 100.0 mL of each metal–ion solutions (0.79 mmol.$L^{-1}$) buffered at pH values from 2.0 to 5.5 were

added. The flaks were transferred to an orbital shaker incubator and stirred at 130 rpm and 25°C until equilibrium was reached. Afterwards, the solids were filtered off through a single filtration and the concentration of each metal ion was determined by FAAS. The maximum pH value of each metal ion solution necessary to avoid the formation of hydrolyzed species and consequent precipitation of metal–ion hydroxides was calculated from the concentration of each metal ion solution and solubility product constant ($K_{sp}$) for $Co(OH)_2$ ($5.92 \times 10^{-15}$), $Cu(OH)_2$ ($1.8 \times 10^{-20}$) and $Ni(OH)_2$ ($5.48 \times 10^{-16}$)[24].

#### 2.3.12.3. Adsorption of metal ions on CTA as a function of initial metal ion concentration

Samples of CTA (20.0 mg) were weighed into 250 mL Erlenmeyer flasks, and 100.0 mL of each metal ion solution, buffered at pH 5.5, with concentrations in the range from 0.05 to 2.42 $mmol.L^{-1}$, were added. The flaks were transferred to an orbital shaker incubator at 25°C and stirred at 130 rpm until equilibrium was reached. Further experimental procedures were equal as those previously described in Sections 2.3.12.1 and 2.3.12.2.

### 2.3.13. Isothermal titration calorimetry (ITC)

The calorimetric experiments were performed in a TAM III isothermal titration nanocalorimeter (TA Instruments, USA) controlled by TAM assistant TM dedicated software. All adsorption measurements were carried out in duplicate at 25.0000 ± 0.0001°C. The equipment has two cells of 4 mL, one for sample and another for reference. The reference cell was filled with 2.7 mL of buffer solution at pH 5.5. The same volume of buffer solution was added to the sample cell containing 0.00700 g of CTA adsorbent. The suspension was stirred at 180 rpm by a propeller stirrer until

thermic equilibrium was reached, when the sample was degassed for 10 min. Afterwards, a monocomponent metal ion solution of $Co^{2+}$, $Cu^{2+}$ or $Ni^{2+}$ buffered at pH 5.5 was added step–wise using a Hamilton syringe of 500 µL controlled by the software. The metal ion concentration in the syringe was 2.20 $mg.L^{-1}$ for $Co^{2+}$, 3.35 $mg.L^{-1}$ for $Cu^{2+}$ and 2.64 $mg.L^{-1}$ for $Ni^{2+}$. The volume of each injection was 15 µL and the time interval between the injections was 35 min. Experiments aiming to evaluate the contribution of the dilution enthalpy of metal ions and CTA adsorbent for the global enthalpy of the process were carried out by metal ion titration in buffer solution without CTA adsorbent and buffer titration in buffer solution containing CTA adsorbent. ITC thermograms were recorded as power against time. The integration of each peak in the ITC thermograms provided the energy in the form of heat absorbed or released after each injection. The changes in adsorption enthalpy ($\Delta_{ads}H°$), for different amounts of metal ion adsorbed, were determined using Eq. (5) as follows:

$$\Delta_{ads}H = \frac{\sum_{i=1}^{m}\left(q_{i,int} - q_{i,dil}\right)}{\sum_{i=1}^{m} n_i} \quad (5)$$

where $q_{i,int}$ and $q_{i,dil}$ are the energies in the form of heat absorbed or released into the sample cell during the $i^{th}$ injection for experiments of metal ion solution titration in buffer solution in the presence or absence of the CTA adsorbent, respectively.

The term $\sum_{i=1}^{m}\left(q_{i,int} - q_{i,dil}\right)$ provides the amount of energy absorbed or released in the adsorption process of $\sum_{i=1}^{m} n_i$ mols of metal ion. The number of mols of adsorbed metal ion after each injection was determined by the adsorption isotherms.

**2.3.14. Approach for calculation of free energy of adsorption**

The changes in free energy of adsorption ($\Delta_{ads}G°$) for the adsorption systems studied can be calculated using Eq. (6) as follows:

$$\Delta_{ads}G° = -RT \ln K_a \quad (6)$$

where $K_a$ is the thermodynamic equilibrium constant (dimensionless), $T$ (K) is the absolute temperature and $R$ is the ideal gas constant (8.314 $J.K^{-1}.mol^{-1}$).

The thermodynamic equilibrium constant can be calculated from the Langmuir constant, $b$, using the approached proposed by Liu [25] as follows:

$$K_a = \left[ \frac{b}{\gamma_e} (1\, mol / L) \right] \quad (7)$$

where $\gamma_e$ is the activity coefficient at equilibrium (dimensionless) at 25°C.

It is well–known that the activity coefficient is strongly affected by the concentration of metal ion solution and it decreases as the ionic strength increases. Thus, it is necessary to correct the activity coefficient for each adsorption system studied using the extended Debye–Hückel law to allow a correct calculation of $\Delta_{ads}G°$ as follows:

$$\log \gamma_e = \frac{-0.509 z^2 \sqrt{I_e}}{1 + \alpha \sqrt{I_e / 305}} \quad (8)$$

where $z$ is the charge of the metal ion, $I_e$ ($mol.L^{-1}$) is the ionic strength at equilibrium, and $\alpha$ (pm) is the hydrated ion size (600 pm for $Co^{2+}$, $Cu^{2+}$ and $Ni^{2+}$).

**2.3.15. Desorption experiments**

Three samples of 70 mg of CTA were weighed into 250 mL Erlenmeyer flasks, and 100.0 mL of each metal ion solution (1.574 $mmol.L^{-1}$ for $Co^{2+}$, $Cu^{2+}$ and $Ni^{2+}$) buffered at pH 5.5 was added. The flasks were placed in an orbital shaker incubator at 25°C and

130 rpm for 180 min. The adsorption parameters used in this study were those considered as optimal in the studies as a function of contact time, solution pH and initial metal ion concentration. Afterwards, the solids were separated by a single filtration, washed with an excess of deionized water to remove unadsorbed metal ions from the CTA adsorbent. Then, CTA–loaded with metal ions was dried at 90°C in an oven for 3 h. The adsorption capacity of CTA for $Co^{2+}$, $Cu^{2+}$ and $Ni^{2+}$ was determined as previously described in Section 2.3.12.1. Three dried samples of 20.0 mg of CTA–loaded with $Co^{2+}$, $Cu^{2+}$ or $Ni^{2+}$ were weighed into 125 mL Erlenmeyer flasks, and 20.0 mL of 1.0 mol.$L^{-1}$ $HNO_3$ was added. The flasks were stirred at 25°C and 130 rpm for 5 min, when the solids were filtered off by a single filtration. The concentration of $Co^{2+}$, $Cu^{2+}$ or $Ni^{2+}$ in the filtrate was determined by FAAS. The solids were washed with an excess of deionized water until neutral pH is reached. The efficiency of desorption ($E_{des}$) was calculated by Eq. (9) as follows [26]:

$$E_{des} / \% = \left( \frac{C_{e,M^{2+}} V_{HNO_3}}{Q_{T,max} w'_{CTA}} \right) \times 100 \quad (9)$$

where $C_{e,M^{2+}}$ (mmol.$L^{-1}$) is the equilibrium concentration of metal ion ($M^{2+}$), $V_{HNO_3}$ (L) is the volume of nitric acid solution, $Q_{T,max}$ (mmol.$g^{-1}$) is the theoretical maximum adsorption capacity determined for each metal ion (as previously described in this Section) and $w'_{CTA}$ (g) is the weight of the CTA adsorbent contained in $w_{CTA,M}^{n+}$. The latter is the weight of the CTA–loaded with $Co^{2+}$, $Cu^{2+}$ or $Ni^{2+}$.

$w'_{CTA}$ can be calculated using Eq. (10) as follows [26]:

$$w'_{CTA} / g = \frac{w_{CTA,M^{n+}} w_{CTA}}{\left( \frac{Q_{T,max} w_{CTA}}{1000} \right) + w_{CTA}} \quad (10)$$

Eq. (10) can be rearranged and simplified, yielding Eq. (11) as follows [26]:

$$w'_{CTA} / g = \frac{w_{CTA,M^{n+}}}{\left(\frac{Q_{T,max}}{1000}\right)+1} \quad (11)$$

### 2.3.16. Reuse of the spent CTA adsorbent

Samples of 20.0 mg of CTA adsorbent recovered from desorption studies were weighed into 250 mL Erlenmeyer flasks, and 100.0 mL of each metal ion solution (0.79 mmol.$L^{-1}$) was added. The optimal experimental conditions determined from adsorption studies were adopted (25°C, 130 rpm, pH 5.5 and 180 min of agitation). Further procedures were the same as those described in Sections 2.3.12.1 and 2.3.12.2. The efficiency of re–adsorption ($E_{re–ads}$) of the CTA adsorbent for one cycle of adsorption–desorption was calculated using Eq. (12) as follows:

$$E_{re\text{-}ads} / \% = \left(\frac{Q_{re\text{-}ads,max}}{Q_{T,max}}\right) \times 100 \quad (12)$$

where $Q_{re–ads,max}$ and $Q_{T,max}$ (mmol.$g^{-1}$) are the maximum adsorption capacities determined in the re–adsorption and adsorption experiments, respectively.

The value of $Q_{re\text{-}ads,max}$ is calculated using Eq. (13) as follows [26]:

$$Q_{re\text{-}ads,max} / \text{mmol/g} = \frac{w'_{M^{n+}} + w''_{M^{n+}}}{w_{CTA}} \quad (13)$$

where $w'_{M}{}^{n+}$ (mg) is the weight of metal ions undesorbed from the CTA adsorbent after desorption and $w''_{M}{}^{n+}$ (mg) is the weight of metal ions adsorbed on the CTA adsorbent in the re-adsorption.

$w'_{M}{}^{n+}$ and $w''_{M}{}^{n+}$ are calculated using Eqs. (14) and (15) as follows [26]:

$$w'_{M^{n+}} = \left[ \left( w_{CTA,M^{n+}} - w'_{CTA} \right) \left( 1 - E_{des}/100 \right) \right] \times 1000 \quad (14)$$

$$w''_{M^{n+}} = \left( C_i - C_e \right) V_{M^{n+}} \quad (15)$$

## 3. Results and discussion

### 3.1. Synthesis and characterization of CTA adsorbent

#### 3.1.1. Percent weight gain and amount of carboxylic acid groups

Figure 1 shows the synthetic route used to prepare the CTA adsorbent, presenting a suggestion of a mechanism through which metal ions ($M^{2+}$) are removed from aqueous solution by the CTA adsorbent, and a suggestion of a desorption mechanism through which metal ions are released from the surface of the CTA adsorbent to the aqueous solution. The chemical modification of C with TA to obtain the CTA adsorbent produces a mixture of two isomers as seen in Figure 1a. These isomers are formed because the hydroxyl groups of C can attack both carbonyl groups of trimellitic anhydride at positions 1 and 2.

The chemical modification of C with TA using Py as a base/catalyst and DMA as a solvent to obtain the CTA (Figure 1a) was extensively studied and optimized through the evaluation of the effects of TA concentration and reaction time on the values of *pwg* and $n_{COOH}$. The results of optimizing the esterification reaction of C with TA are shown in Table 1, which shows that as the TA amount was augmented for a reaction time of 1 h, *pwg* and $n_{COOH}$ also augmented. In order to better explore the effect of reaction time on *pwg* and $n_{COOH}$, amounts of 4.71 and 9.48 g of TA were chosen for subsequent studies. For both amounts of TA (4.71 and 9.48 g) as the reaction time was increased, *pwg* and $n_{COOH}$ also increased. However, as the degree of modification of cellulose is increased, a tendency of formation of a gel is observed as a consequence of the esterification of secondary hydroxyl groups at C–2 and C–3, which increases the

distance between cellulose chains due to the great size of trimellitate moiety. Thus, in view of such a problem, exploratory tests of adsorption of $Cu^{2+}$ on some CTA adsorbents prepared were performed in order to understand the behavior of the CTA adsorbent in aqueous solution during the adsorption process. These testes aimed choosing the best CTA adsorbent in terms of adsorption capacity, behavior in aqueous solution during the adsorption process, i.e. solubility and swelling, and the cost of preparation of the adsorbent material. As seen in Table 1, the exploratory tests for $Cu^{2+}$ adsorption on CTA adsorbents showed that the adsorption capacities ($Q_{max}$) for the adsorbents tested were similar. Moreover, the CTA adsorbent that exhibited the best behavior in aqueous solution was that prepared using 7.11 g of TA and 1 h of reaction time. Thus, this CTA adsorbent was chosen for the subsequent experiments of adsorption of $Co^{2+}$, $Cu^{2+}$ and $Ni^{2+}$ in aqueous solution.

When increasing the reaction scale to 8.0 g of C and 56.93 g TA, the *pwg* and $n_{COOH}$ values were 94.5% and 6.81 ± 0.02 mmol.$g^{-1}$, respectively. The scale–up of the reaction resulted in a decrease in the *pwg* by 30.3% and an increase in $n_{COOH}$ by 37.6%. However, the *pwg* decreased in the scale–up of the reaction, there was an increase in $n_{COOH}$, which is the most important parameter for a material regarding its use as an adsorbent for heavy metal ions. The estimated preparation cost of the CTA adsorbent (TA/C ratio = 6:1 and 1 h reaction time) based on the international market prices of the chemicals used and electricity in Brazil was US$ 77.45 per kg of CTA. The preparation cost of the CTA did not take into account the chemicals used in the elaboration steps (Section 2.2.1) and the possibility of recovering and recycling solvents and excess of TA. In comparison with STA adsorbent (sugarcane bagasse modified with trimellitic anhydride) prepared by Ramos, Xavier, Teodoro, Elias, Gonçalves, Gil, Freitas and Gurgel [5], which cost US$ 57.43 per kg of STA, there was an increase of US$ 20.02

per kg of adsorbent or 34.9%. The difference in the preparation costs for both adsorbent materials has also to be evaluated in terms of their performances in the adsorption process to allow a better understanding. The STA adsorbent exhibited maximum experimental adsorption capacities ($Q_{max,exp}$) for $Co^{2+}$, $Cu^{2+}$ and $Ni^{2+}$ of 0.950, 1.121 and 1.295 mmol.g$^{-1}$, respectively [5]. As will be presented in section 3.4.3, $Q_{max,exp}$ of the CTA adsorbent for $Co^{2+}$, $Cu^{2+}$ and $Ni^{2+}$ were 0.749, 1.487 and 1.001 mmol.g$^{-1}$. The adsorption capacities for $Co^{2+}$ and $Ni^{2+}$ of the STA adsorbent were 26.8% and 29.4% higher than those of the CTA adsorbent, whereas for $Cu^{2+}$ $Q_{max,exp}$ of the CTA was 32.7% higher than that of the STA adsorbent. This means that in terms of economic analysis, the CTA adsorbent is only economically feasible for adsorption of $Cu^{2+}$ in comparison with STA adsorbent.

### 3.1.2. Elemental analysis, FTIR and $^{13}$C SS NMR spectroscopy

Elemental analysis was performed for C and CTA. The carbon, hydrogen and nitrogen contents for C and CTA were 44.45 and 46.55%, 6.22 and 4.40, and 0.00 and 0.49%, respectively. Figure 2a presents the FTIR spectra for C and CTA. The main changes noticed in the spectrum of C in comparison with CTA are: (1) the increase in the bandwidth related to the stretching of O–H groups at 3300–3400 cm$^{-1}$ due to the introduction of trimellitate moiety; (2) the appearance of bands at 2638 and 2522 cm$^{-1}$ corresponding to the stretching of hydrogen bonding exhibited by dimers of aromatic carboxylic acid; (3) a strong band at 1718 cm$^{-1}$ related to the stretching of conjugated carbonyl ester, which often overlaps the band related to the stretching of carbonyl of carboxylic acid; (4) bands at 1612 and 1492 cm$^{-1}$ due to the stretching of C=C bonds in the benzene ring of trimellitate moiety; (5) a band at 1282 cm$^{-1}$ related to the stretching of C–O of ester and 752 cm$^{-1}$ corresponding to the C–H out–of–plane bending of 1,2,4–substituted benzenoid ring [27]. The absence of bands at 1850–1800 cm$^{-1}$ related

to asymmetric and symmetric stretching of carbonyl of cyclic carboxylic acid anhydride in the spectrum of the CTA indicates that this material is free of unreacted TA.

Figure 2b shows the FTIR spectra for the CTA and CTA–loaded with $Co^{2+}$, $Cu^{2+}$ and $Ni^{2+}$. The adsorption of $Co^{2+}$, $Cu^{2+}$ and $Ni^{2+}$ on the CTA was characterized by the splitting of the band in the region of 1685 $cm^{-1}$, which corresponds to the stretching of carbonyl of carboxylic acid groups. This band appears to be overlapped by a broad band centered at 1718 $cm^{-1}$. After adsorption takes place, this band is split into two broad bands at 1592 and 1552 $cm^{-1}$, which correspond to the asymmetric stretching of carboxylate groups [28], thereby indicating that carboxylate groups are involved in the adsorption of metal ions as suggested in Figure 1b.

Figure 3a and b shows the $^{13}C$ SS NMR spectra of C and CTA. The signal at 64 ppm is related to carbon at C–6, whereas the signal between 70 and 74 ppm is related to carbons at C–2, C–3 and C–5 and at 88 and 103 ppm corresponds to the carbons at C–4 and C–1 of the β–D–anhydroglucopyranose unit (AGU), respectively [29]. The main changes in the spectrum of the CTA in comparison with C are: (1) the appearance of a broad signal centered at 131 ppm, which is attributed to carbons from C–7 to C–12 of the aromatic ring of trimellitate moiety and (2) a broad signal centered at 167 ppm, which is attributed to carbons at C–13, C–14 and C–15 of the ester and carboxylic acid groups [27]. The signals centered at 200 and 58 ppm are assigned as spinning sidebands related to the method of signal acquisition.

### 3.1.3. Thermogravimetric analysis

TGA and DTG curves for thermal decomposition of C and CTA are shown in Supplementary Figure 1a and b. The first weight loss for thermal decomposition of C and CTA occurred at 50°C and 63°C, respectively, which can be related to the

vaporization of bound water. The thermal decomposition of C exhibited a single main decomposition event with a maximum decomposition temperature ($T_m$) at 377°C, whereas the thermal decomposition of CTA presented two main decomposition events with maximum decomposition temperatures ($T_{m,1}$ and $T_{m,2}$) at 268°C and 323°C, respectively. The initial ($T_i$) and onset ($T_{onset}$) decomposition temperatures for C were 187°C and 338°C. For CTA, $T_{i,1}$ and $T_{i,2}$ were 141°C and 298°C, whereas $T_{onset}$ was 235°C. A comparison between thermal decomposition temperatures ($T_i$, $T_{onset}$ and $T_m$) for C and CTA showed that chemical modification of C with TA decreased the thermal stability of the resulting material (CTA). It also suggests that the introduction of trimellitate moiety into cellulose structure decreased the cohesive forces between cellulose chains maintained by intermolecular hydrogen bonds, which is the major responsible, along with degree of crystallinity and polymerization, for cellulose thermal stability [30]. The decrease in the thermal stability of cellulose esters such as cellulose succinate and cellulose benzoate in comparison with unmodified cellulose was also reported by Sairam, Sreedhar, Mohan Rao and Palaniappan [31].

### 3.1.4. XRD analysis

The XRD patterns of C and CTA are presented in Supplementary Figure 2a and b. Unmodified C exhibited the typical pattern of cellulose I with the main diffraction signals at 2θ 15.2, 16.7, 23.0 and 34.6°, which are commonly attributed to the diffraction planes 101, $10\bar{1}$, 002 and 040, respectively [32]. The diffractogram of the CTA presented the same typical XRD pattern of cellulose I (at 2θ 14.9, 16.5, 22.7 and 34.3°) and no peak shifting or appearance of new peaks was noticed. Moreover, the chemical modification seems to have occurred at the cellulose fiber surface and amorphous regions of cellulose without strongly affecting the ultrastructure of the fibers, the degree of crystallinity of cellulose decreased after chemical modification

from 51.8% to 34.4%. Similar observations were made by Jandura, Kokta and Riedl [33] for modification of cellulose with unsaturated and saturated organic acids with 11 and 18 carbons, respectively, and are attributed to slight rearrangements of cellulose chains caused by the incorporation of large derivatization reagents.

### 3.2. SEM analysis

SEM was used to assess the morphological changes in the surface of C after chemical modification with TA. Figure 4a–d presents SEM images of C and CTA at 200 × (a and b) and 10,000 × (c and d). As seen in Figure 4a and b, the fibrous aspect of CTA was preserved after chemical modification in comparison with C, which demonstrates that chemical modification occurred at the surface of cellulose fibers, thereby corroborating with DRX data. As seen Figure 4c and d, the surface of the CTA fiber shows some fissures and cell walls are not intact in comparison with surface of C. The exposure of primary and secondary cell walls seems to be increased after chemical modification with TA, suggesting that modification with a large organic ligand probably increased the separation of cellulose chains. However, appearance of holes was not observed on the CTA surface, which could favor the diffusion of metal ions into CTA adsorbent structure.

### 3.3. Analysis of specific surface area and pore size distribution of CTA adsorbent

The textural properties of the CTA adsorbent were calculated by BET and BJH methods. CTA adsorbent presented a specific surface area of 3.196 ± 0.217 $m^2.g^{-1}$, an average micropores size of 38.30 ± 0.13 Å, a total pores volume of 0.0038 ± 0.0002 $cm^3.g^{-1}$, a maximum pores diameter of 570.95 ± 38.25 Å and an average pores size of 23.73 ± 0.44 Å. According to the International Union of Pure and Applied Chemistry (IUPAC), porous materials can be classified into three categories: pores < 20 Å in

diameter are micropores, pores between 20-500 Å are mesopores and pores > 500 Å are macropores [34]. Then, CTA adsorbent can be classified as a mesoporous material.

### 3.4. Adsorption experiments

#### 3.4.1. Effect of the solution pH on metal ion removal

The influence of the solution pH on metal ion removal on the CTA adsorbent was evaluated at 25°C and 130 rpm with a 0.79 mmol.$L^{-1}$ metal ion solution and 0.2 g.$L^{-1}$ CTA as well as 180 min equilibrium time ($t_e$). The $t_e$ was based on kinetic data for adsorption of $Co^{2+}$, $Cu^{2+}$ and $Ni^{2+}$ on the CTA adsorbent as seen in Table 2. Figure 5 shows the equilibrium adsorption capacity ($q_e$) of $Co^{2+}$, $Cu^{2+}$ and $Ni^{2+}$ on the CTA adsorbent as a function of the solution pH from 2.0 to 5.75. The influence of the solution pH on metal ion adsorption is related to the net surface charge of the CTA adsorbent as well as the form of metal ions in solution. The net surface charge of an adsorbent material in aqueous solution is related to its PZC value. The PZC value determined for the CTA adsorbent was 2.80 ± 0.09. Therefore, the adsorption of metal ions is favored at pH > PCZ, where the surface of the CTA is negatively charged due to the deprotonation of carboxylic acid groups of trimellitate moiety. As seen in Figure 5, $q_e$ increased as the solution pH increased. At low pH values (pH < 2.80), carboxylic groups on the CTA adsorbent are protonated and no adsorption of metal ions on the CTA adsorbent took place. From pH values slightly higher than PZC, the adsorption took place as a consequence of strong attraction between negatively charged carboxylate groups ($–COO^-$) present in the surface of the CTA and cationic metal ions ($M^{2+}$) in aqueous solution. The maximum $q_e$ value was attained at pH 5.5 for $Co^{2+}$, $Cu^{2+}$ and $Ni^{2+}$. Adsorption at pH values higher than 5.75 was not evaluated, as the formation of metal–hydrolyzed species [$M(OH)^+$] may occur with consequent precipitation of metal–ion hydroxide [$M(OH)_{2(s)}$]. Thus, a pH value of 5.5 was considered as the

optimum pH value for adsorption of $Co^{2+}$, $Cu^{2+}$ and $Ni^{2+}$ on the CTA adsorbent for the subsequent adsorption studies as a function of contact time and initial metal ion concentration.

### 3.4.2. Adsorption kinetics

The adsorption kinetics is one of the most important parameters for designing a wastewater treatment plant (WWTP) operating in batch and semicontinuous adsorption mode [35].

The pseudo–first–order (PFO) equation developed by Lagergren [36] for the adsorption of oxalic and malonic acids onto charcoal describes the rate of adsorption in the liquid–phase systems. The PFO equation in its differential form is written as follows [37]:

$$\frac{dq(t)}{dt} = k_1\left(q_e - q(t)\right) \tag{16}$$

where $q_e$ and $q_t$ (mmol.g$^{-1}$) are the adsorption capacities at equilibrium ($t_e$) and at time $t$ (min), respectively, and $k_1$ (min$^{-1}$) is the PFO rate constant for the kinetic model. When solving and rearranging Eq. (16) using the boundary conditions of $q_t = 0$ at $t = 0$ and $q_t = q_t$ at $t = t$, yields:

$$q_t = q_e\left(1 - \exp^{-k_1 t}\right) \tag{17}$$

Ho and McKay [38] described a kinetic process of the adsorption of divalent metal ions onto peat, in which the chemical bonding among divalent metal ions and polar functional groups on peat surface are responsible for the cation–exchange capacity of the peat [37]. In the pseudo–second–order (PSO) kinetic model the amount of divalent

metal ions adsorbed on the surface of the adsorbent at a time $t$ and at equilibrium ($t_e$) is represented as follows:

$$\frac{dq(t)}{dt} = k_2 \left(q_e - q(t)\right)^2 \tag{18}$$

where the driving force of the adsorption process, ($q_e - q(t)$), is proportional to the available fraction of active adsorption sites and $k_2$ (g.mmol$^{-1}$.min$^{-1}$) is the PSO rate constant for the kinetic model. When solving and rearranging Eq. (18) using the boundary conditions of $q_t = 0$ at $t = 0$ and $q_t = q_t$ at $t = t$, yields:

$$q_t = \frac{k_2 q_e^{\,2} t}{1 + k_2 q_e t} \tag{19}$$

The model of Boyd, Adamson and Myers [39] and Weber and Morris [40] are widely used for evaluating the adsorption mechanism. The model of Boyd [39] determines if the major resistance to mass transfer is in the thin film named boundary layer, which surrounds the adsorbent particle, or in the resistance to diffusion inside the pores [41]. The model is presented as follows:

$$f = 1 - \frac{6}{\pi^2} \sum_{n=1}^{\infty} \frac{1}{n^2} \exp\left(-n^2 Bt\right) \tag{20}$$

where $f$ is the fractional loading ($f = q_t/q_e$) as a function of time and $Bt$ is a function of $f$. By applying the Fourier transform in Eq. (20), Reichenberg [42] obtained approximations that allow him to solve Eq. (20) as follows:

$$\text{For } f \text{ values} > 0.85 \quad Bt = -0.4977 - \ln\left(1 - f\right) \tag{21}$$

$$\text{and for } f \text{ values} < 0.85 \quad Bt = \left(\sqrt{\pi} - \sqrt{\pi - \frac{\pi^2 f}{3}}\right)^2 \tag{22}$$

$B$ can be used to calculate the effective diffusion coefficient, $D_i$ ($cm^2.s^{-1}$), from the Eq. (23) as follows:

$$B = \frac{\pi^2 D_i}{r^2} \tag{23}$$

where $r$ is the radius of the CTA adsorbent particle (average diameter of 0.250 mm) [41].

Eqs. (21)-(23) can be used to predict the adsorption mechanism by plotting a graph of $Bt$ against $t$. If the plot yields a straight line which passes through the origin, then pore diffusion controls the mass transfer rate (MTR). If the plot yields a linear or non-linear curve which does not passes through the origin, then it is suggested that film diffusion controls the adsorption rate of metal ions on the CTA adsorbent [41].

Weber and Morris [40] derivate a pore diffusion model from Fick's second diffusion law [41]. The model is presented as follows:

$$q_t = k_i t^{1/2} + C \tag{24}$$

where $k_i$ ($mmol.g^{-1}.min^{-1/2}$) is the intraparticle diffusion rate constant and $C$ is the intercept, which may suggest the thickness of boundary layer. The larger the value of $C$ the greater is the boundary layer effect. If the plot of $q_t$ against $t^{1/2}$ yields a straight line that crosses the origin ($C = 0$), then pore diffusion is the sole rate-limiting step controlling the adsorption mechanism, while if the plot yields a straight line that does not cross from the origin ($C \neq 0$) or the plot is multilinear and the first linear portion does not cross the origin, then the process controlling the adsorption mechanism can be film diffusion and pore diffusion simultaneously.

The kinetic models of PFO and PSO were used to model the adsorption rate of metal ions on the surface of the CTA adsorbent at pH 5.5, 25°C, 130 rpm, 0.79 mmol.$L^{-1}$ metal ion solution and 0.2 g.$L^{-1}$ CTA adsorbent with agitation times ranging from 2 to 600 min, while models of Boyd, Adamson and Myers [39] and Weber and Morris [40] were used to evaluate the adsorption mechanism. The experimental kinetic data were modeled by nonlinear regression analysis (NLR) using Microcal OriginPro® 2015 software, which was set to use PFO [Eq. (17)] and PSO [Eq. (19)] models, the Levenberg–Marquardt iteration algorithm and the weight method named statistical [Eq. (25)]. In this method, the weights are used to minimize the chi–square ($\chi^2$) value [Eq. (26)] to obtain the best fitting curve. The coefficient of determination ($R^2$) and reduced chi–square ($\chi^2_{red}$) [Eq. (27)] were used to evaluate the quality of the NRL and to define the best kinetic model describing the adsorption rate of $Co^{2+}$, $Cu^{2+}$ and $Ni^{2+}$ on the CTA adsorbent.

$$w_i = \frac{1}{y_i} \tag{25}$$

where $w_i$ is the weighting coefficient and $y_i$ is the experimental data point.

$$\chi^2 = \sum_{i=1}^{N} w_i \left( y_i - \hat{y}_i \right)^2 \tag{26}$$

where $\hat{y}_i$ is the estimated data point calculated by the model (PFO or PSO).

$$\chi^2_{red} = \frac{\chi^2}{\upsilon} \tag{27}$$

where $\chi^2_{red}$ is the reduced chi–squared and $\upsilon$ is the number of degrees of freedom ($\upsilon = N - P$), which depends on the number of experimental data points ($N$) and number of variables ($P$) of the PFO and PSO models.

Table 2 shows the estimated kinetic parameters obtained by modeling the experimental kinetic data with PFO and PSO models using NLR analysis. Experimental kinetic data are available in Supplementary Table 1 (see the Supplementary Material). Supplementary Figure 3a–c shows graphs of $q_t$ against $t$ for the adsorption of $Co^{2+}$, $Cu^{2+}$ and $Ni^{2+}$ on the CTA adsorbent, and the curves fitted to the experimental kinetic data using the PFO and PSO models are also shown. As seen in Table 2, the model that best described the adsorption rate of $Co^{2+}$ and $Cu^{2+}$ on the CTA adsorbent was the PFO model (higher $R^2$ and smaller $\chi^2_{red}$), while the adsorption rate of $Ni^{2+}$ on the CTA adsorbent was best described by the PSO model (higher $R^2$ and smaller $\chi^2_{red}$). In addition, when the values of experimental adsorption capacity ($q_{e,exp}$) are compared to the values of estimated adsorption capacity ($q_{e,est}$), it is noticed that the values of $q_{e,est}$ estimated by the PFO for $Co^{2+}$ and $Cu^{2+}$ were closer to those of $q_{e,exp}$, whereas for $Ni^{2+}$ the value of $q_{e,est}$ estimated by the PSO was closer to that of $q_{e,exp}$. As seen in Supplementary Figure 3a–c, the values of equilibrium adsorption capacity ($q_e$) were attained at 70 min for $Co^{2+}$, $Cu^{2+}$ and $Ni^{2+}$, respectively.

Supplementary Figure 4a-c shows the intraparticle diffusion plot for $Co^{2+}$, $Cu^{2+}$ and $Ni^{2+}$ adsorption on the CTA adsorbent. These plots are multilinear and the first portion did not cross the origin, thereby indicating that adsorption rate is controlled by film diffusion for all metal ions and then changed to intraparticle diffusion until equilibrium for $Co^{2+}$ and $Ni^{2+}$ [43]. The intraparticle diffusion plots indicates two stages for $Cu^{2+}$ and three stages for $Co^{2+}$ and $Ni^{2+}$. Table 2 shows the intraparticle diffusion coefficients ($k_i$) for $Co^{2+}$, $Cu^{2+}$ and $Ni^{2+}$. Supplementary Figure 5d-f shows the Boyd plots for $Co^{2+}$, $Cu^{2+}$ and $Ni^{2+}$ adsorption on the CTA adsorbent. The slopes ($B$) obtained from linear portions were used to calculate the effective diffusion coefficient ($D_i$) [43], which are presented in Table 2. The Boyd plots were linear in the initial adsorption period and did

not cross the origin. However, the values of $B$ were closer to zero, indicating that external mass transfer is the rate-limiting step controlling the adsorption of $Cu^{2+}$ and the major part of the adsorption of $Co^{2+}$ and $Ni^{2+}$.

### 3.4.3. Adsorption isotherms

Adsorption isotherms can describe the phenomenon governing the removal of an adsorbate from an aqueous medium to a solid–phase at a constant temperature and pH [44]. Thus, adsorption isotherms are of fundamental importance in the design of batch or semicontinuous adsorption systems in a WWTP [5].

The Freundlich isotherm model [45], which is the oldest known relationship describing the non–ideal and reversible adsorption, is not limited to the formation of a monolayer. In addition, this model can be applied to multilayer adsorption, with non–uniform distribution of adsorption heat and affinities over the heterogeneous surface [44]. The Freundlich isotherm is given by Eq. (28):

$$q_e = K_F C_e^{1/n} \tag{28}$$

where $q_e$ (mmol.g$^{-1}$) is the equilibrium adsorption capacity, $C_e$ (mmol.L$^{-1}$) is the metal ion equilibrium concentration in the aqueous solution, $K_F$ [(mmol.g$^{-1}$)(L.mmol$^{-1}$)$^{1/n}$] is the Freundlich constant and $n$ is a parameter indicative of adsorption intensity or surface heterogeneity.

The Langmuir isotherm model [46] was originally developed to describe the adsorption on gas–solid phase. This empirical model assumes the formation of a monolayer with adsorption occurring at a finite number of fixed localized binding sites, which are identical and equivalent, with no adsorbate–adsorbate interaction and steric hindrance between the adsorbed molecules, even on adjacent binding sites. The model refers to

homogeneous adsorption where each molecule possesses constant enthalpy and activation energy of adsorption [44]. The Langmuir model is given by Eq. (29):

$$q_e = \frac{Q_{max} b C_e}{1 + b C_e} \quad (29)$$

where $Q_{max}$ (mmol.g$^{-1}$) is the maximum adsorption capacity and $b$ (L.mmol$^{-1}$) is the Langmuir binding constant related to the energy involved in adsorption.

The Sips isotherm model [47] is a combination of the Langmuir and Freundlich isotherm models deduced for predicting the heterogeneous adsorption systems and outwitting the limitation of the increasing adsorbate concentration related to the Freundlich isotherm model. At low adsorbate concentrations, it is reduced to the Freundlich isotherm; while at high concentrations, it is reduced to the Langmuir isotherm. The Sips model is given by Eq. (30):

$$q_e = Q_{max} \frac{(b C_e)^{1/n}}{1 + (b C_e)^{1/n}} \quad (30)$$

Adsorption isotherms of $Co^{2+}$, $Cu^{2+}$ and $Ni^{2+}$ on the CTA adsorbent were performed at 25°C, 130 rpm, pH 5.5, 0.2 g.L$^{-1}$ CTA and 0.05–1.36 mmol.L$^{-1}$ metal ion solution, with an equilibrium time of 70 min (based on the kinetic data of Section 3.4.2). Table 3 presents the estimated parameters obtained by modeling the experimental adsorption data (Supplementary Table 2) with the Langmuir, Freundlich and Sips models through NLR analysis using Microcal OriginPro® 2015 software as previously described in Section 3.4.2. Supplementary Figure 6a–c presents graphs of $q_e$ against $C_e$ for the adsorption of $Co^{2+}$, $Cu^{2+}$ and $Ni^{2+}$ on the CTA adsorbent, and the curves fitted to the experimental data using the isotherm models. As seen in Table 3, the model that best described the adsorption of $Co^{2+}$, $Cu^{2+}$ and $Ni^{2+}$ on the CTA adsorbent was the

Langmuir model, which exhibited the higher values of $R^2$ and smaller values of $\chi^2_{red}$. As the Sips model is an equation of three parameters contrary to the Langmuir and Freundlich equations, which have two parameters, it has more degrees of freedom; and in the minimization procedure used to solve the equations by maximizing the value of $R^2$ and minimizing the value of $\chi^2$ this model will fit better the experimental data in comparison with the Langmuir and Freundlich models. Because of that, the Sips model was only used to evaluate the heterogeneity of the adsorbent surface. As seen in Table 3, the adsorption systems formed by CTA–$Co^{2+}$ and CTA–$Cu^{2+}$ were more heterogeneous than that formed by CTA–$Ni^{2+}$, considering the values of the parameter *n* of the Sips model. Moreover, the CTA adsorbent was prepared from pure cellulose material and presents only carboxylic groups from trimellitate moiety as metal ligands, it possesses carboxyl groups exhibiting different values of p$K_a$ and such groups can still present different conformations for metal binding [48]. Therefore, based on the values of the parameter *n* of the Sips model and the values of $R^2$ and $\chi^2_{red}$, it is suggested that the adsorption systems can be approached by the Langmuir model, even that the presence of adsorption sites exhibiting possible different affinities toward metal ions studied may occur due to different conformations adopted by the ligands on the CTA surface (see Figure 1a for the possibility of formation two isomers in the preparation of the CTA adsorbent).

According to experimental equilibrium data ($Q_{max,exp}$) and the Langmuir model ($Q_{max,est}$), the maximum metal ion adsorption capacity of the CTA adsorbent exhibited the following order $Cu^{2+}$ > $Ni^{2+}$ > $Co^{2+}$, whereas the Langmuir binding constant presented the following order $Cu^{2+}$ > $Co^{2+}$ > $Ni^{2+}$.

### 3.5. Energy dispersive X–ray (EDX) spectroscopy

EDX spectroscopy was used to map the distribution of the adsorbed metal ions along the adsorption surface sites of the CTA adsorbent. Figure 6a–c shows the distribution of $Co^{2+}$, $Cu^{2+}$ and $Ni^{2+}$ on the surface of the CTA adsorbent. As seen in Figure 6a–c, a uniform distribution of adsorbed $Co^{2+}$, $Cu^{2+}$ and $Ni^{2+}$ was observed along the surface of the CTA adsorbent, which suggests the formation of a uniform layer of the metal ions on the CTA adsorbent surface. This is in agreement with the Langmuir theory, which was the best isotherm model describing the adsorption of $Co^{2+}$, $Cu^{2+}$ and $Ni^{2+}$ on the CTA surface.

### 3.6. Thermodynamics of adsorption

#### 3.6.1. Isothermal titration calorimetry

Isothermal titration calorimetry (ITC) allows to accurately measure the energy as the heat associated to the system composition changes during the titration process [49]. Thus, titration of the metal ion solution in a dispersion containing the CTA adsorbent enables to determine the enthalpic contribution to the transferring process of metal ions from the bulk solution to the adsorbent surface. Supplementary Figure 7 shows the enthalpy of adsorption as a function of the amount of metal ions adsorbed in the equilibrium on the CTA surface.

As seen in Supplementary Figure 7, the curves presented similar profiles, indicating that the adsorption mechanism is the same for all metal ions studied. Furthermore, it seen that the values of $\Delta_{ads}H$ are positive and vary title with the increase of $q_e$, being that the greater variation of $\Delta_{ads}H$ was observed for $Cu^{2+}$ adsorption (0.5 $kJ.mol^{-1}$). A slight difference may occur due to the different conformations adopted by the carboxylic ligands on the CTA surface. These results indicate that the energy of interaction of the metal ions with each adsorption site on the CTA surface is close and confirm the earlier assumptions that experimental adsorption data fitted well to the Langmuir model.

The values of $\Delta_{ads}H°$ were positive, thus indicating that the adsorption process is endothermic. In order to better understand the adsorption mechanism and the driving force governing the adsorption process is necessary to evaluate the enthalpic contribution of each subprocess occurring simultaneously when the metal ions migrate from the bulk solution to the CTA surface.

The value of $\Delta_{ads}H°$ is a result of the contribution of three subprocesses: *i*) desolvation of metal ions and anions from the CTA surface ($\Delta_{desol}H^{\text{CTA sites,metal ions}}$), *ii*) metal ion–metal ion interactions ($\Delta_{int}H^{\text{metal-metal}}$) and *iii*) CTA site–metal ion interactions ($\Delta_{int}H^{\text{CTA sites-metal ions}}$). Thus, the enthalpy of adsorption is the sum of these three contributions and can be presented by Eq. (31) as follows:

$$\Delta_{ads}H° = \Delta_{desol}H^{\text{CTA sites,metal ions}} + \Delta_{int}H^{\text{metal-metal}} + \Delta_{int}H^{\text{CTA sites-metal ions}} \quad (31)$$

The contribution of the subprocess *i* for $\Delta_{ads}H°$ can be evaluated from the value of $\Delta_{desol}H$ of each metal ion. These values are positive and contribute to the adsorption process to be exothermic [50]. The metal ion–metal ion interactions, subprocess *ii*, also increase the enthalpy of the system, but this contribution is less significant than the others, since the enthalpy values do not vary significantly with increasing concentration of the metal ions. The CTA site–metal ion interactions, subprocess *iii*, contributes to a decrease in the enthalpy of the system, i.e., energy is released as metal ions interact with the adsorption sites present on the surface of the CTA adsorbent.

Since the values of $\Delta_{ads}H°$ for adsorption of $Co^{2+}$, $Cu^{2+}$ and $Ni^{2+}$ on the CTA adsorbent are positive, the energies released from subprocesses *iii* are smaller than the energies involved in the desolvation of metal ions and anions on the CTA surface (subprocesses *i*) and the repulsive interactions between metal–metal on the CTA surface (subprocesses *ii*).

### 3.6.2. Thermodynamic analysis of the systems

The thermodynamic parameter, $\Delta_{ads}G°$, is the result of the enthalpic and entropic contributions. Therefore, in order to elucidate the mechanism of adsorption of metal ions on the CTA surface is necessary to evaluate each contribution individually. The variation of the standard enthalpy of adsorption ($\Delta_{ads}H°$) was determined from a curve of $\Delta_{ads}H$ as a function of $C_e$, extrapolating $C_e$ tending to zero. The values of $\Delta_{ads}H°$ are presented in Table 4. The entropic contribution, $\Delta_{ads}S°$, was determined from the classical thermodynamic relationship given by Eq. (32) as follows:

$$\Delta_{ads}G° = \Delta_{ads}H° - T\Delta_{ads}S° \quad (32)$$

Table 4 shows the values of the standard thermodynamic properties for adsorption of $Co^{2+}$, $Cu^{2+}$ and $Ni^{2+}$ on the CTA adsorbent. The values of $\Delta_{ads}G°$ were negative for all metal ions studied, thereby showing the spontaneity of the adsorption process. In addition, the values $\Delta_{ads}H°$ were positive, which indicate that the adsorption process is endothermic and entropically directed. This is confirmed by the values of the term $T\Delta_{ads}S°$, which shows that migration of metal ions from bulk solution to the CTA surface causes an increase in the entropy of the system. The entropic contribution can be attributed to the water molecules that are released from desolvation of the metal ions and adsorption sites on the CTA surface.

### 3.7. Desorption

The CTA adsorbent loaded with metal ions was desorbed using an aqueous 1.0 $mol.L^{-1}$ $HNO_3$ solution at 25°C and 130 rpm for 5 min. Table 3 presents the desorption efficiencies for the CTA adsorbent loaded with $Co^{2+}$, $Cu^{2+}$ and $Ni^{2+}$. As seen in Table 3, the desorption efficiencies ($E_{des}$) were close to 100% for all metal ions loaded on the CTA adsorbent, showing that it is possible to recover both the CTA adsorbent and metal

ions, which certainly improves the economic feasibility for the application of the CTA adsorbent in processes for treating contaminated water by heavy metal ions. At pH equals to zero, there is a high concentration of hydronium ions, which may be exchanged by metal ions through the protonation of carboxylate groups in the trimellitate moiety, thereby suggesting that ion–exchange is the main mechanism controlling the desorption of metal ions from the CTA adsorbent surface, as presented in Figure 1c.

### 3.8. Re–adsorption

The re–adsorption studies were performed using the CTA adsorbents that were desorbed with 1.0 mol.$L^{-1}$ $HNO_3$ for 5 min. The re–adsorption efficiencies ($E_{re–ads}$) for $Co^{2+}$, $Cu^{2+}$ and $Ni^{2+}$ were close to 100% as can be seen in Table 3. These results suggest that the CTA adsorbent can be recovered and reused without significant loss of the adsorption capacity.

### 3.9. Comparison with literature data for $Co^{2+}$, $Cu^{2+}$ and $Ni^{2+}$ adsorption on different adsorbent materials

Table 5 presents different adsorbent materials that have been used to remove $Co^{2+}$, $Cu^{2+}$ and $Ni^{2+}$ from aqueous solutions, as reported in the literature, for comparison purposes. A comparison of CTA adsorbent with those reported in the literature shows that the CTA adsorbent is among the most powerful adsorbents prepared for this purpose, and therefore, is a promising adsorbent material because it is from a renewable source and can be fully desorbed and reused without a significant decrease in its adsorption capacity.

## 4. Conclusions

The synthesis of cellulose trimellitate (CTA) was accomplished and optimized. The best CTA adsorbent was obtained with a percent weight gain, number of carboxylic acid groups and point of zero charge of 94.5%, 6.81 mmol.g$^{-1}$, and 2.80, respectively. Adsorption studies as a function of the solution pH, time and initial metal ion concentration were developed. The pH of maximum adsorption capacity ($Q_{max}$) for $Co^{2+}$, $Cu^{2+}$ and $Ni^{2+}$ was 5.5. The adsorption of $Co^{2+}$ and $Cu^{2+}$ followed the pseudo-second-order kinetic model, whereas the adsorption of $Ni^{2+}$ followed the pseudo-first-order model. The adsorption systems were best described by the Langmuir model with $Q_{max}$ of 0.749, 1.487 and 1.001 mmol.g$^{-1}$ for $Co^{2+}$, $Cu^{2+}$ and $Ni^{2+}$, respectively. A mixed adsorption mechanism was suggested as ion–exchanged followed by complexation of metal ions by carboxylate groups. Thermodynamic data showed that the adsorption is entropically driven. Desorption and re–adsorption studies showed that the CTA adsorbent can be fully desorbed and reused without loss in its adsorption capacity.

**Acknowledgements**

The authors are grateful to Universidade Federal de Ouro Preto (UFOP grant number 23.109.006271/2014–70) and Fundação de Amparo à Pesquisa do Estado de Minas Gerais (FAPEMIG grant number APQ–01945/13) for funding this research. The authors are also grateful to Coordenação de Aperfeiçoamento de Pessoal de Nível Superior (CAPES). The authors would like to acknowledge the Nanolab Electronic Microscopy Laboratory, at the Redemat, Escola de Minas, UFOP, MG, Brazil, for providing the equipment and technical support for experiments involving electron microscopy and B. S. Ney P. Sampaio for SEX–EDX analyses and Prof. Eduardo Ribeiro de Azevêdo for the analyses of $^{13}C$ SS NMR. This work is a collaboration research project of members of the Rede Mineira de Química (RQ–MG) supported by FAPEMIG (Project: CEX – RED–00010–14).

**References**

[1] M. Ahmaruzzaman, Industrial wastes as low-cost potential adsorbents for the treatment of wastewater laden with heavy metals, Adv. Colloid Interface Sci. 166(1–2) (2011) 36-59.

[2] P.O. Boamah, Y. Huang, M. Hua, Q. Zhang, J. Wu, J. Onumah, L.K. Sam-Amoah, P.O. Boamah, Sorption of heavy metal ions onto carboxylate chitosan derivatives—A mini-review, Ecotoxicol. Environ. Saf. 116(0) (2015) 113-120.

[3] M. Salman, M. Athar, U. Farooq, Biosorption of heavy metals from aqueous solutions using indigenous and modified lignocellulosic materials, Rev Environ Sci Biotechnol 14(2) (2015) 211-228.

[4] M.A. Barakat, New trends in removing heavy metals from industrial wastewater, Arabian J. Chem. 4(4) (2011) 361-377.

[5] S.N.C. Ramos, A.L.P. Xavier, F.S. Teodoro, M.M.C. Elias, F.J. Gonçalves, L.F. Gil, R.P. Freitas, L.V.A. Gurgel, Modeling mono-and multi-component adsorption of cobalt (II), copper (II), and nickel (II) metal ions from aqueous solution onto a new carboxylated sugarcane bagasse. Part I: Batch adsorption study, Ind. Crop. Prod. 74 (2015) 357-371.

[6] D.W. O'Connell, C. Birkinshaw, T.F. O'Dwyer, Heavy metal adsorbents prepared from the modification of cellulose: A review, Bioresour. Technol. 99(15) (2008) 6709-6724.

[7] ATSDR, Support document to the 2013 priority list of hazardous substances that will be the subject of toxicological profiles, Division of Toxicology and Environmental Medicine, Atlanta, GA, 2014, pp. 1-12.

[8] P. Ahmad, N.V. Prasad, Environmental adaptations and stress tolerance of plants in the era of climate change, Springer New York, 2011.

[9] F. Fu, Q. Wang, Removal of heavy metal ions from wastewaters: A review, J. Environ. Manage. 92(3) (2011) 407-418.

[10] A. Abdolali, W.S. Guo, H.H. Ngo, S.S. Chen, N.C. Nguyen, K.L. Tung, Typical lignocellulosic wastes and by-products for biosorption process in water and wastewater treatment: A critical review, Bioresour. Technol. 160 (2014) 57-66.

[11] L.V.A. Gurgel, O.K. Junior, R.P.D.F. Gil, L.F. Gil, Adsorption of Cu(II), Cd(II), and Pb(II) from aqueous single metal solutions by cellulose and mercerized cellulose chemically modified with succinic anhydride, Bioresour. Technol. 99(8) (2008) 3077-3083.

[12] M. Vandenbossche, M. Jimenez, M. Casetta, M. Traisnel, Remediation of Heavy Metals by Biomolecules: A Review, Crit. Rev. Env. Sci. Technol. 45(15) (2014) 1644-1704.

[13] M. Ahmad, S. Ahmed, B.L. Swami, S. Ikram, Adsorption of heavy metal ions: Role of chitosan and cellulose for water treatment, Int. J. Pharmacogn. 2(6) (2015) 280-289.

[14] R. Saravanan, L. Ravikumar, The Use of New Chemically Modified Cellulose for Heavy Metal Ion Adsorption and Antimicrobial Activities, J. Water Resour. Prot. 7(06) (2015) 530.

[15] D. Klemm, B. Heublein, H.P. Fink, A. Bohn, Cellulose: fascinating biopolymer and sustainable raw material, Angew. Chem. Int. Edit. 44(22) (2005) 3358-3393.

[16] A.P. Mariano, M.O.S. Dias, T.L. Junqueira, M.P. Cunha, A. Bonomi, R.M. Filho, Butanol production in a first-generation Brazilian sugarcane biorefinery: Technical aspects and economics of greenfield projects, Bioresour. Technol. 135 (2013) 316-323.

[17] Y.G. Ko, A.D. Khasbaatar, U.S. Choi, J.-Y. Kim, Molecular interaction mechanism in solid polymer electrolyte comprising cellulose phthalate and $LiClO_4$, Solid State Ionics 181(25–26) (2010) 1178-1182.

[18] J.S. Noh, J.A. Schwarz, Effect of $HNO_3$ treatment on the surface-acidity of activated carbons, Carbon 28(5) (1990) 675-682.

[19] R.C. Sun, Cereal straw as a resource for sustainable biomaterials and biofuels: chemistry, extractives, lignins, hemicelluloses and cellulose, 1st ed., Elsevier, Oxford, UK, 2010.

[20] R.L. Johnson, K. Schmidt-Rohr, Quantitative solid-state 13C NMR with signal enhancement by multiple cross polarization, J. Magn. Reson. 239 (2014) 44-49.

[21] J. Guo, J.M. Catchmark, Surface area and porosity of acid hydrolyzed cellulose nanowhiskers and cellulose produced by Gluconacetobacter xylinus, Carbohydr. Polym. 87(2) (2012) 1026-1037.

[22] S. Brunauer, P.H. Emmett, E. Teller, Adsorption of Gases in Multimolecular Layers, J. Am. Chem. Soc. 60(2) (1938) 309-319.

[23] E.P. Barrett, L.G. Joyner, P.P. Halenda, The Determination of Pore Volume and Area Distributions in Porous Substances. I. Computations from Nitrogen Isotherms, J. Am. Chem. Soc. 73(1) (1951) 373-380.

[24] W.M. Haynes, CRC Handbook of Chemistry and Physics, 95th ed., Taylor & Francis, 2014.

[25] Y. Liu, Is the Free Energy Change of Adsorption Correctly Calculated?, J. Chem. Eng. Data 54(7) (2009) 1981-1985.

[26] F.T.R.d. Almeida, B.C.S. Ferreira, A.L.d.S.L. Moreira, R.P.d. Freitas, L.F. Gil, L.V.A. Gurgel, Application of a new bifunctionalized chitosan derivative with zwitterionic characteristics for the adsorption of $Cu^{2+}$, $Co^{2+}$, $Ni^{2+}$, and oxyanions of $Cr^{6+}$ from aqueous solutions: Kinetic and equilibrium aspects, J Colloid Interf Sci 466 (2016) 297-309.

[27] D. Pavia, G. Lampman, G. Kriz, J. Vyvyan, Introduction to Spectroscopy, 4th ed., Cengage Learning, 2014.

[28] R. Łyszczek, Thermal and spectroscopic investigations of new lanthanide complexes with 1,2,4-benzenetricarboxylic acid, J. Therm. Anal. Calorim. 90(2) (2007) 533-539.

[29] K. Kamide, K. Okajima, K. Kowsaka, T. Matsui, CP/MASS 13C NMR Spectra of Cellulose Solids: An Explanation by the Intramolecular Hydrogen Bond Concept, Polym J 17(5) (1985) 701-706.

[30] L.V.A. Gurgel, K. Marabezi, L.A. Ramos, A.A.d.S. Curvelo, Characterization of depolymerized residues from extremely low acid hydrolysis (ELA) of sugarcane bagasse cellulose: Effects of degree of polymerization, crystallinity and crystallite size on thermal decomposition, Ind. Crop. Prod. 36(1) (2012) 560-571.

[31] M. Sairam, B. Sreedhar, D.V. Mohan Rao, S. Palaniappan, Synthesis and thermal degradation kinetics of cellulose esters, Polymers for Advanced Technologies 14(7) (2003) 477-485.

[32] C.S.R. Freire, A.J.D. Silvestre, C.P. Neto, M.N. Belgacem, A. Gandini, Controlled heterogeneous modification of cellulose fibers with fatty acids: Effect of reaction conditions on the extent of esterification and fiber properties, J. Appl. Polym. Sci. 100(2) (2006) 1093-1102.

[33] P. Jandura, B.V. Kokta, B. Riedl, Fibrous long-chain organic acid cellulose esters and their characterization by diffuse reflectance FTIR spectroscopy, solid-state CP/MAS 13C-NMR, and X-ray diffraction, J. Appl. Polym. Sci. 78(7) (2000) 1354-1365.

[34] J. Rouquerol, D. Avnir, C. Fairbridge, D. Everett, J. Haynes, N. Pernicone, J. Ramsay, K. Sing, K. Unger, Recommendations for the characterization of porous solids (Technical Report), Pure Appl. Chem. 66(8) (1994) 1739-1758.

[35] Y.S. Ho, G. McKay, Pseudo-second order model for sorption processes, Process Biochem. 34(5) (1999) 451-465.

[36] S.Y. Lagergren, Zur Theorie der sogenannten Adsorption gelöster Stoffe, Kungliga Svenska Vetenskapsakademiens, Handlingar 24(4) (1898) 1-39.

[37] H. Qiu, L. Lv, B.-c. Pan, Q.-j. Zhang, W.-m. Zhang, Q.-x. Zhang, Critical review in adsorption kinetic models, J. Zhejiang Univ. Sci. A 10(5) (2009) 716-724.

[38] Y. Ho, G. McKay, Kinetic model for lead (II) sorption on to peat, Adsorpt Sci Technol 16(4) (1998) 243-255.

[39] G.E. Boyd, A.W. Adamson, L.S. Myers, The Exchange Adsorption of Ions from Aqueous Solutions by Organic Zeolites. II. Kinetics1, J. Am. Chem. Soc. 69(11) (1947) 2836-2848.

[40] W.J. Weber, J.C. Morris, Kinetics of adsorption on carbon from solution, J. San. Eng. Div. 89(2) (1963) 31-60.

[41] B.H. Hameed, M.I. El-Khaiary, Malachite green adsorption by rattan sawdust: Isotherm, kinetic and mechanism modeling, J. Hazard. Mater. 159(2–3) (2008) 574-579.

[42] D. Reichenberg, Properties of Ion-Exchange Resins in Relation to their Structure. III. Kinetics of Exchange, J. Am. Chem. Soc. 75(3) (1953) 589-597.

[43] B.H. Hameed, M.I. El-Khaiary, Batch removal of malachite green from aqueous solutions by adsorption on oil palm trunk fibre: Equilibrium isotherms and kinetic studies, J. Hazard. Mater. 154(1–3) (2008) 237-244.

[44] K.Y. Foo, B.H. Hameed, Insights into the modeling of adsorption isotherm systems, Chem. Eng. J. 156(1) (2010) 2-10.

[45] H.M.F. Freundlich, Over the adsorption in solution, Z Phys Chem-Stoch Ve 57(4) (1906) 385-470.

[46] I. Langmuir, The adsorption of gases on plane surfaces of glass, mica and platinum, J. Am. Chem. Soc. 40(9) (1918) 1361-1403.

[47] R. Sips, On the Structure of a Catalyst Surface, J. Chem. Phys. 16(5) (1948) 490-495.

[48] T. Anirudhan, P. Suchithra, Equilibrium, kinetic and thennodynamic modeling for the adsorption of heavy metals onto chemically modified hydrotalcite, Indian J. Chem. Techn. 17(4) (2010) 247-259.

[49] J.-P.E. Grolier, J.M. del Río, Isothermal titration calorimetry: A thermodynamic interpretation of measurements, J. Chem. Thermodyn. 55 (2012) 193-202.

[50] Y. Marcus, The thermodynamics of solvation of ions. Part 2.-The enthalpy of hydration at 298.15 K, J. Chem. Soc., Faraday Trans. 1 F 83(2) (1987) 339-349.

[51] S.N.d.C. Ramos, A.L.P. Xavier, F.S. Teodoro, L.F. Gil, L.V.A. Gurgel, Removal of cobalt(II), copper(II), and nickel(II) ions from aqueous solutions using phthalate-functionalized sugarcane bagasse: Mono- and multicomponent adsorption in batch mode, Ind. Crop. Prod. 79 (2016) 116-130.

[52] S.N.d.C. Ramos, A.L.P. Xavier, F.S. Teodoro, M.M.C. Elias, F.J. Gonçalves, L.F. Gil, R.P. de Freitas, L.V.A. Gurgel, Modeling mono- and multi-component adsorption of cobalt(II), copper(II), and nickel(II) metal ions from aqueous solution onto a new carboxylated sugarcane bagasse. Part I: Batch adsorption study, Ind. Crop. Prod. 74 (2015) 357-371.

[53] I.G. Shibi, T.S. Anirudhan, Kinetic and equilibrium modeling of adsorption of cobalt(II) from aqueous solutions onto surface modified lignocellulosics (Musa paradisiaca), Indian J. Chem. Techn. 13 (2006) 567-575.

[54] J.C.P. de Melo, E.C. da Silva Filho, S.A.A. Santana, C. Airoldi, Maleic anhydride incorporated onto cellulose and thermodynamics of cation-exchange process at the solid/liquid interface, Colloid and Surface A 346(1-3) (2009) 138-145.

[55] L.V. Gurgel, O.K. Junior, R.P. Gil, L.F. Gil, Adsorption of Cu(II), Cd(II), and Pb(II) from aqueous single metal solutions by cellulose and mercerized cellulose chemically modified with succinic anhydride, Bioresour. technol. 99(8) (2008) 3077-83.

[56] J. Li, S. Zhang, C. Chen, G. Zhao, X. Yang, J. Li, X. Wang, Removal of Cu(II) and fulvic acid by graphene oxide nanosheets decorated with Fe3O4 nanoparticles, ACS Appl Mater Interfaces 4(9) (2012) 4991-5000.

[57] O. Karnitz, Jr., L.V.A. Gurgel, R.P. de Freitas, L.F. Gil, Adsorption of Cu(II), Cd(II), and Pb(II) from aqueous single metal solutions by mercerized cellulose and mercerized sugarcane bagasse chemically modified with EDTA dianhydride (EDTAD), Carbohydrate Polymers 77(3) (2009) 643-650.

[58] J. Li, C. Chen, S. Zhang, X. Ren, X. Tan, X. Wang, Critical evaluation of adsorption-desorption hysteresis of heavy metal ions from carbon nanotubes: influence of wall number and surface functionalization, Chem Asian J 9(4) (2014) 1144-51.

[59] S. Yang, C. Chen, Y. Chen, J. Li, D. Wang, X. Wang, W. Hu, Competitive Adsorption of $Pb^{II}$, $Ni^{II}$, and $Sr^{II}$ Ions on Graphene Oxides: A Combined Experimental and Theoretical Study, ChemPlusChem 80(3) (2015) 480-484.

[60] C. Chen, X. Wang, Adsorption of Ni(II) from Aqueous Solution Using Oxidized Multiwall Carbon Nanotubes, Ind. Eng. Chem. Res. 45 (2006) 9144-9149.

**Figure 1.** (a) Scheme illustrating the synthetic route used to obtain the CTA adsorbent (R = H or trimellitate group), (b) suggested mechanism for removal of metal ions ($M^{2+}$) on the CTA adsorbent [M = Co, Cu, or Ni and $mX^{n-}$ = counter ion ($SO_4^{2-}$, $Cl^-$ or $CH_3COO^-$)], and (c) suggested desorption mechanism of the metal ions from surface of the CTA adsorbent.

**Figure 2.** FTIR spectra of (a) C and (b) CTA and CTA loaded with $Co^{2+}$, $Cu^{2+}$, and $Ni^{2+}$ (transmittances of CTA–$Co^{2+}$, CTA–$Cu^{2+}$, and CTA–$Ni^{2+}$ spectra were shifted by 15, 30, and 45% in relation to the CTA spectrum).

**Figure 3.** $^{13}C$ SS NMR spectra of (a) C and (b) CTA (* represents spinning sidebands).

**Figure 4.** SEM images of C (a and c) and CTA (b and d) at 200× and 10,000× magnification.

**Figure 5.** Effect of the solution pH on the adsorption of $Co^{2+}$, $Cu^{2+}$, and $Ni^{2+}$ onto the CTA (0.79 $mmol.L^{-1}$ $M^{2+}$, 130 rpm, 25°C, 0.2 $g.L^{-1}$ CTA and 180 min of shaking for $Co^{2+}$, $Cu^{2+}$, and $Ni^{2+}$, respectively).

**Figure 6.** SEM–EDX images with surface mapping for (a) $Co^{2+}$, (b) $Cu^{2+}$, and (c) $Ni^{2+}$ adsorbed on the CTA adsorbent surface.

**Table 1.** The results of optimizing esterification of C with TA to obtain CTA.

**Table 2.** Results of nonlinear regression analysis of the experimental kinetic data for the adsorption of metal ions on the CTA (0.79 $mmol.L^{-1}$ $M^{2+}$, pH = 5.5, 25°C, 130 rpm, 0.2 $g.L^{-1}$ SPA).

**Table 3.** Results of modeling the equilibrium adsorption data with three isotherm models (25°C, 130 rpm, pH 5.5, and 0.2 $g.L^{-1}$ CTA).

**Table 4.** Thermodynamics parameters of adsorption of $Co^{2+}$, $Cu^{2+}$, and $Ni^{2+}$ on the CTA adsorbent at 25°C (298 K).

**Table 5.** Comparison of different adsorbent materials reported in the literature for removal of $Co^{2+}$, $Cu^{2+}$ and $Ni^{2+}$ from aqueous solutions.

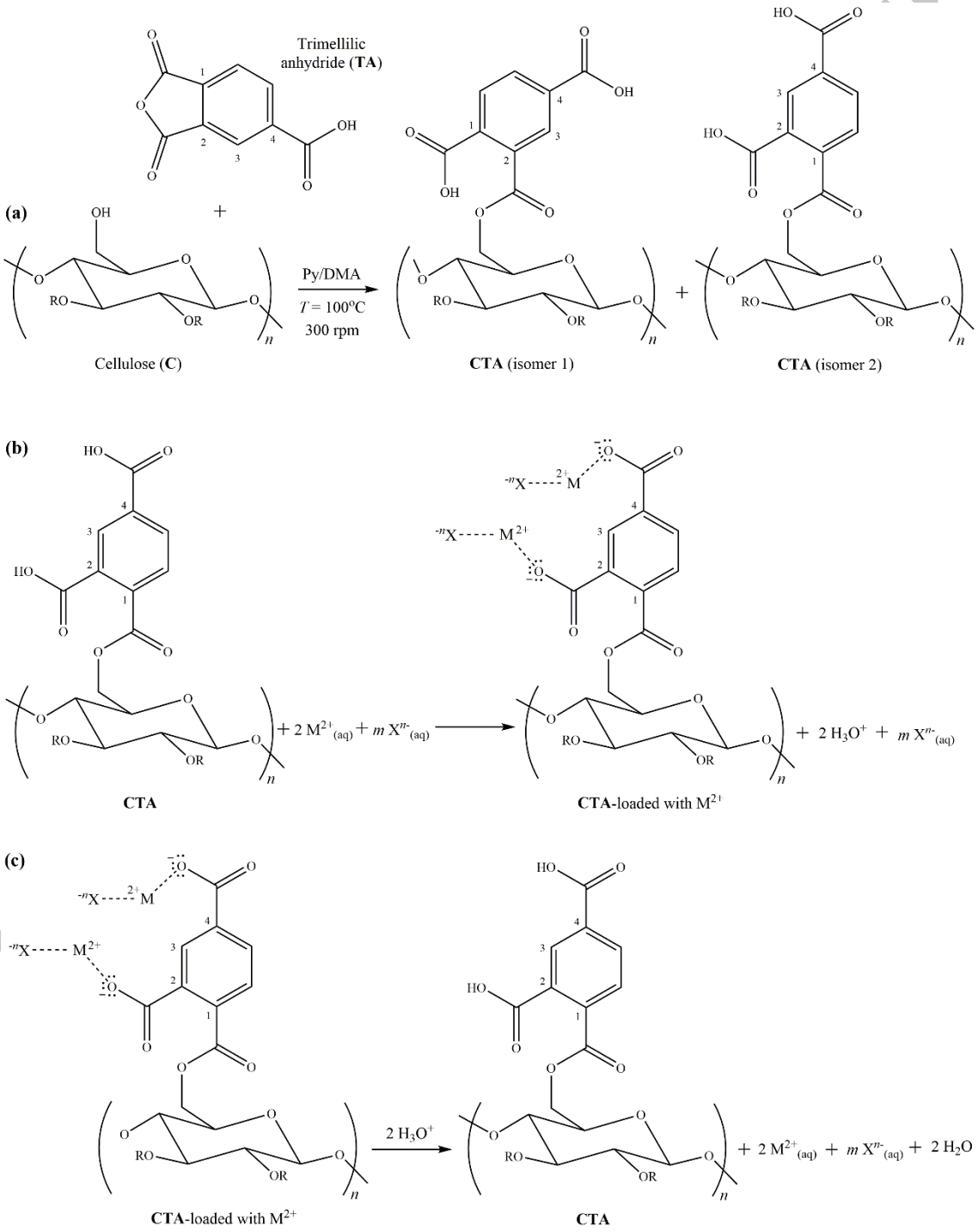


**Figure 1.**

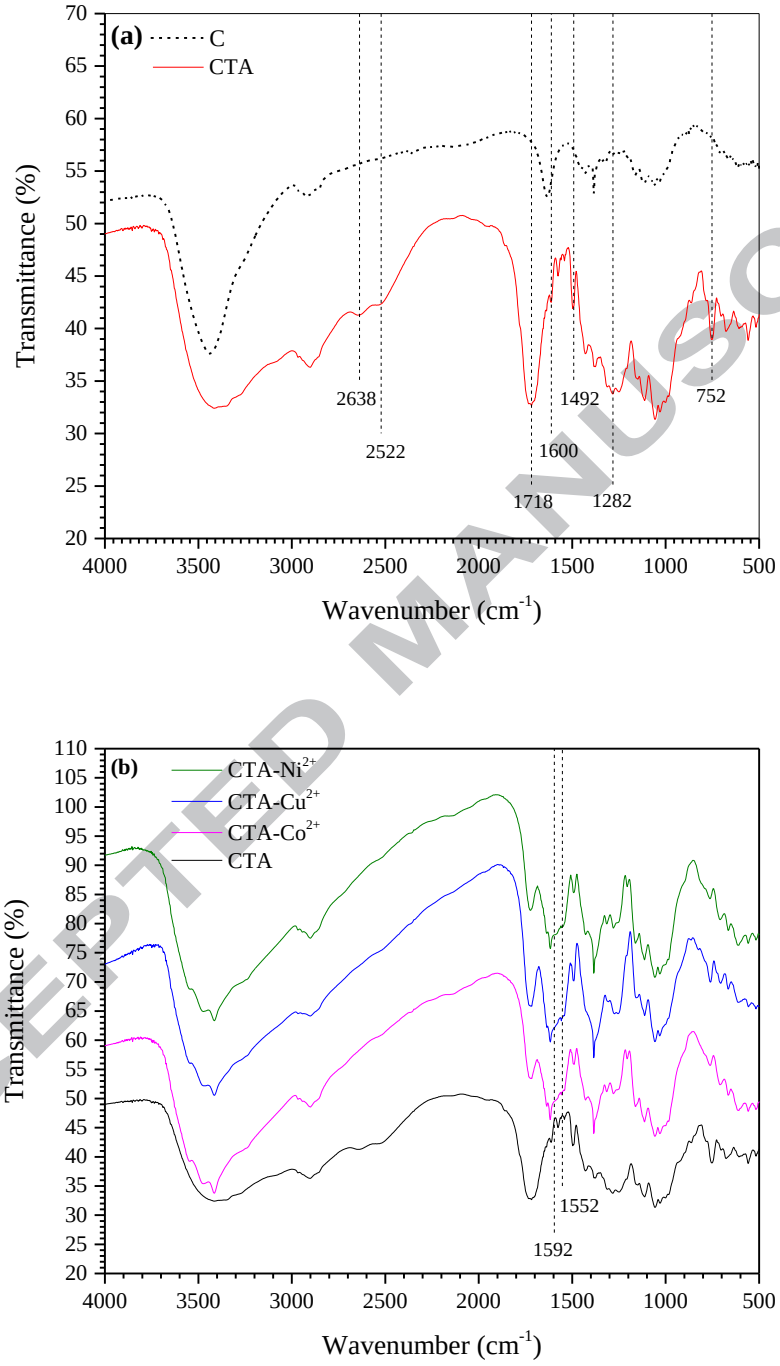


**Figure 2.**

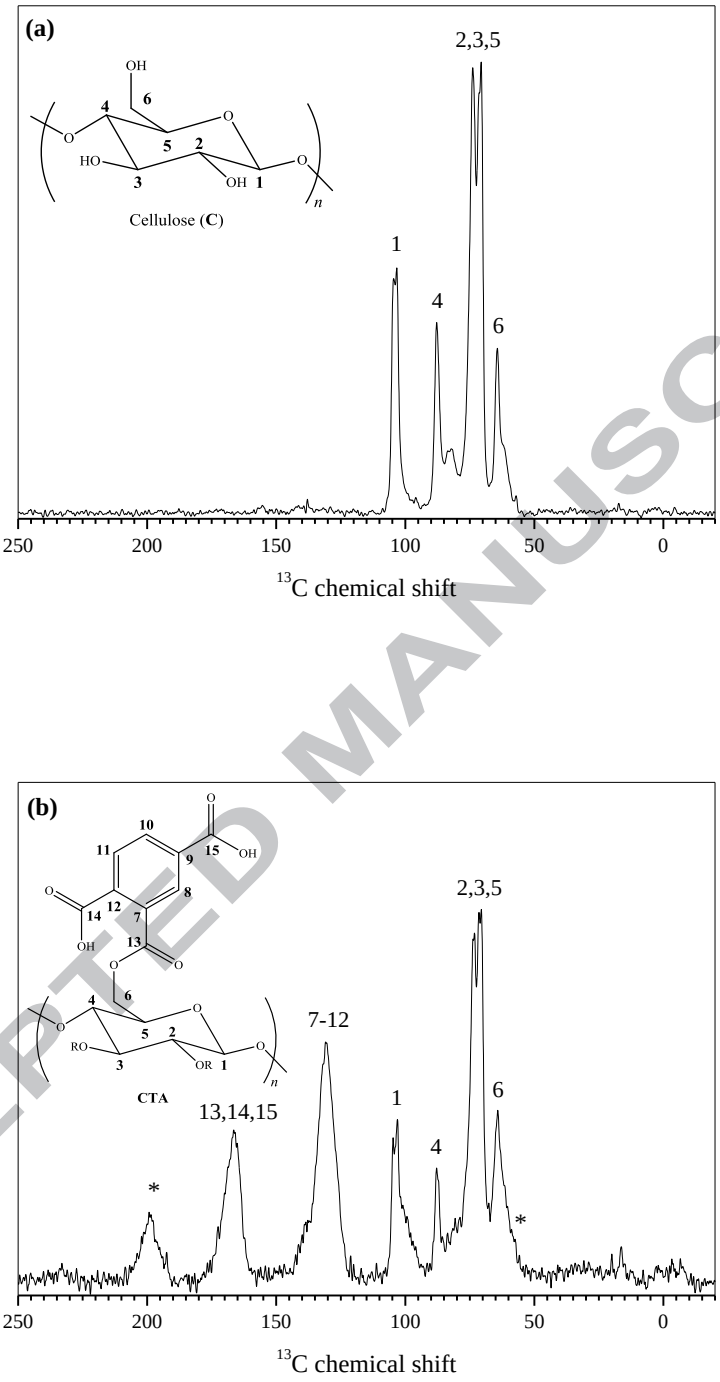


**Figure 3.**

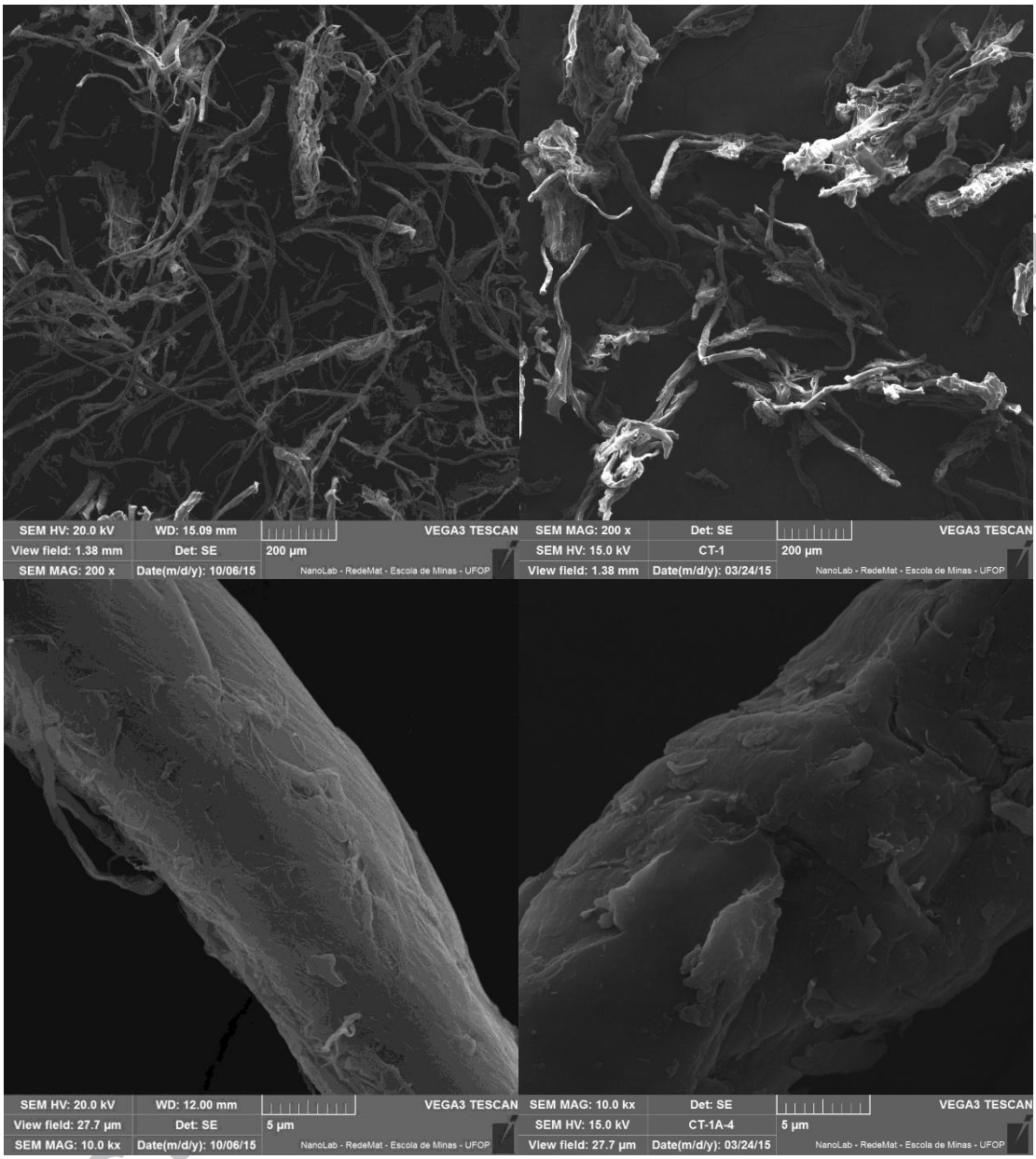
SEM HV: 20.0 kV
WD: 15.09 mm
VEGA3 TESCAN
View field: 1.38 mm
Det: SE
200 µm
SEM MAG: 200 x
Date(m/d/y): 10/06/15
NanoLab - RedeMat - Escola de Minas - UFOP
SEM MAG: 200 x
Det: SE
VEGA3 TESCAN
SEM HV: 15.0 kV
CT-1
200 µm
View field: 1.38 mm
Date(m/d/y): 03/24/15
NanoLab - RedeMat - Escola de Minas - UFOP
SEM HV: 20.0 kV
WD: 12.00 mm
VEGA3 TESCAN
View field: 27.7 µm
Det: SE
5 µm
SEM MAG: 10.0 kx
Date(m/d/y): 10/06/15
NanoLab - RedeMat - Escola de Minas - UFOP
SEM MAG: 10.0 kx
Det: SE
VEGA3 TESCAN
SEM HV: 15.0 kV
CT-1A-4
5 µm
View field: 27.7 µm
Date(m/d/y): 03/24/15
NanoLab - RedeMat - Escola de Minas - UFOP

**Figure 4.**

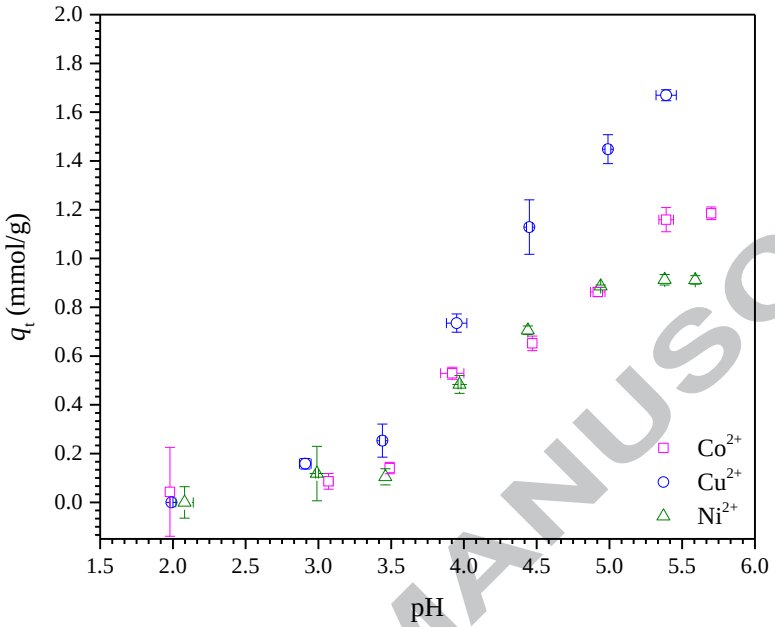


**Figure 5.**

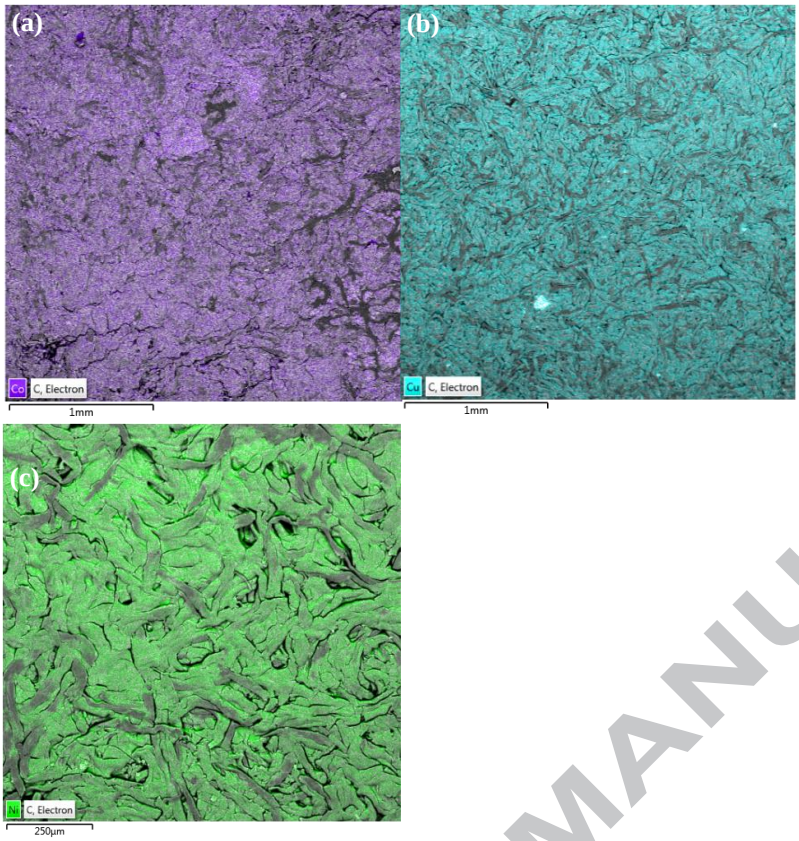


**Figure 6.**

**Table 1.**

| Trimellitic anhydride (TA)[a] (g) | Reaction time (h) | CTA[b] | | $Q_{max}$ (mmol.g$^{-1}$)[c] for $Cu^{2+}$ |
|---|---|---|---|---|
| | | *pwg* (%) | $n_{COOH}$ (mmol.g$^{-1}$) | |
| 2.37 | 1 | 47.1 ± 2.8 | 3.01 ± 0.18 | – |
| 4.74 | | 96.8 ± 1.4 | 4.57 ± 0.03 | – |
| 7.11 | | 123.1 ± 5.7 | 4.95 ± 0.01 | 0.604 ± 0.033 |
| 9.48 | | 150.0 ± 7.6 | 5.34 ± 0.08 | – |
| 4.74 | 0.5 | 59.3 ± 0.0 | 5.03 ± 0.10 | – |
| | 1 | 96.8 ± 1.4 | 4.57 ± 0.03 | – |
| | 3 | 149.0 ± 0.0 | 6.55 ± 0.07 | – |
| 9.48 | 0.5 | 124.4 ± 14.1 | 5.79 ± 0.47 | – |
| | 0.75 | 131.2 ± 8.7 | 5.43 ± 0.34 | – |
| | 1 | 150.0 ± 7.6 | 5.34 ± 0.08 | 0.544 ± 0.026 |
| | 2 | 183.4 ± 30.3 | 6.58 ± 0.11 | 0.658 ± 0.013 |
| | 3 | 268.5 ± 16.3 | 6.55 ± 0.26 | – |

[a] The weights of TA (192.13 g.mol$^{-1}$) were calculated with basis on the equivalents of TA (2, 4, 6, and 8 equivalents of TA per mol of AGU (162.14 g.mol$^{-1}$)) for 1.0 g of starting material (6.17 mmols);
[b] The weight of C used in all chemical modifications was 1.0 g. All reactions were performed in duplicate.
[c] The adsorption conditions were not optimized for these tests of $Cu^{2+}$ adsorption (pH = 5.5; $T$ = 25°C, $t$ = 6 h, [$Cu^{2+}$] = 1.57 mmol.L$^{-1}$, $m_{ads}$ = 0.0200 g).

**Table 2.**

| Parameters/metals | $Co^{2+}$ | $Cu^{2+}$ | $Ni^{2+}$ |
|---|---|---|---|
| $t_e$ (min) | 70 | 70 | 70 |
| $q_{e.exp}$ (mmol.g$^{-1}$) | 0.960 ± 0.030 | 1.446 ± 0.019 | 1.014 ± 0.037 |
| Pseudo–first–order | | | |
| $q_{e.est}$ (mmol.g$^{-1}$) | 0.952 ± 0.012 | 1.474± 0.020 | 0.989 ± 0.028 |
| $k_1$ (min$^{-1}$) | (1.329 ±0.061) × 10$^{-1}$ | (1.191 ± 0.067) × 10$^{-1}$ | (2.442 ± 0.370) × 10$^{-1}$ |
| $R^2$ | 0.9934 | 0.9905 | 0.8127 |
| $\chi^2_{red}$ | 0.0013 | 0.0029 | 0.0081 |
| Pseudo–second–order | | | |
| $q_{e.est}$ (mmol.g$^{-1}$) | 1.010 ± 0.021 | 1.570 ± 0.055 | 1.039 ± 0.017 |
| $k_2$ (g.mmol$^{-1}$.min$^{-1}$) | (1.725 ± 0.173) × 10$^{-1}$ | (1.017 ± 0.193) × 10$^{-1}$ | (3.899 ± 0.486) × 10$^{-1}$ |
| $R^2$ | 0.9837 | 0.9467 | 0.9454 |
| $\chi^2_{red}$ | 0.0033 | 0.0161 | 0.0024 |
| Intraparticle diffusion | | | |
| *Step1* | | | |
| $k_{i,1}$ (mmol.g$^{-1}$.min$^{-1/2}$) | 0.204± 0.023 | 0.417± 0.039 | 0.141± 0.003 |
| $C$ (mmol.g$^{-1}$) | -0.0051± 0.074 | -0.282± 0.088 | 0.325± 0.010 |
| $R^2$ | 0.9511 | 0.9573 | 0.9982 |
| *Step2* | | - | |
| $k_{i,2}$ (mmol.g$^{-1}$.min$^{-1/2}$) | 0.0037± 0.0019 | - | 0.019± 0.004 |
| $C$ (mmol.g$^{-1}$) | 0.919± 0.020 | - | 0.872± 0.031 |
| $R^2$ | 0.4709 | - | 0.8645 |
| Boyd plot | | | |
| $B$ | 0.033± 0.006 | 0.042± 0.007 | 0.060± 0.008 |
| $D_i$ (cm$^2$.s$^{-1}$) | 5.224 × 10$^{-7}$ | 6.700 × 10$^{-7}$ | 9.531 × 10$^{-7}$ |

**Table 3.**

| Isotherm models | Parameters | $Co^{2+}$ | $Cu^{2+}$ | $Ni^{2+}$ |
|---|---|---|---|---|
| Experimental data | $Q_{max.exp}$ (mmol.g$^{-1}$) | 0.749 ± 0.013 | 1.487 ± 0.027 | 1.001 ± 0.002 |
| | $t_e$ (min) | 70 | 70 | 70 |
| | $I_e$ (mol.L$^{-1}$) | 0.0515 | 0.0542 | 0.0531 |
| | $\gamma_e$ | 0.886 | 0.886 | 0.886 |
| Langmuir | $Q_{max.est}$ (mmol.g$^{-1}$) | 0.878 ± 0.015 | 1.683 ± 0.027 | 1.199 ± 0.036 |
| | $b$ (L.mmol$^{-1}$) | 5.85 ± 0.28 | 10.98 ± 0.65 | 3.87 ± 0.28 |
| | $R^2$ | 0.9944 | 0.9847 | 0.9939 |
| | $\chi^2_{red}$ | 0.0008 | 0.0015 | 0.0023 |
| Freundlich | $K_F$ [mmol.g$^{-1}$/(L.mmol$^{-1}$)$^{1/n}$] | 0.714 ± 0.034 | 1.527 ± 0.050 | 0.897 ± 0.041 |
| | $n$ | 2.90 ± 0.28 | 4.60 ± 0.50 | 2.50 ± 0.21 |
| | $R^2$ | 0.9005 | 0.8900 | 0.9191 |
| | $\chi^2_{red}$ | 0.0141 | 0.0106 | 0.0015 |
| Sips | $Q_{max.est}$ (mmol.g$^{-1}$) | 0.844 ± 0.020 | 1.665 ±0.053 | 1.231 ± 0.078 |
| | $b$ (L.mmol$^{-1}$) | 6.50 ± 0.42 | 11.12 ± 0.76 | 3.60 ± 0.60 |
| | $n$ | 0.91 ± 0.05 | 0.96 ± 0.11 | 1.04 ± 0.09 |
| | $R^2$ | 0.9956 | 0.9849 | 0.9881 |
| | $\chi^2_{red}$ | 0.0007 | 0.0016 | 0.0009 |
| Desorption | $E_{des}$ (%) | 97.31 ± 0.19 | 100.31 ± 1.12 | 98.81 ± 1.36 |
| Re–adsorption | $E_{re–ads}$ (%) | 96.12 | 97.53 | 97.79 |

**Table 4.**

| Thermodynamics parameters | $Co^{2+}$ | $Cu^{2+}$ | $Ni^{2+}$ |
|---|---|---|---|
| $\Delta_{ads}G°$ (kJ.mol$^{-1}$) | -21.80 ± 1.04 | -23.36 ± 1.39 | -20.78 ± 1.50 |
| $\Delta_{ads}H°$ (kJ.mol$^{-1}$) | 6.25 ± 0.03 | 8.09 ± 0.02 | 5.36 ± 0.14 |
| $T\Delta_{ads}S°$ (kJ.mol$^{-1}$) | 28.05 ± 1.07 | 31.45 ± 1.40 | 26.13 ± 1.64 |

**Table 5.**

| Adsorbent | Modification | Metal ion | $Q_{max}$ (mmol.g$^{-1}$) | pH | Adsorbent dosage (g/L) | Agitation speed (rpm) | $T$ ($^{o}$C) | Reference |
|---|---|---|---|---|---|---|---|---|
| Sugar cane bagasse | Phthalic anhydride | $Co^{2+}$ | 0.462 | 5.75 | 0.2 | 130 | 25 | [51] |
| Sugar cane bagasse | Trimellitic anhydride | $Co^{2+}$ | 0.950 | 5.75 | 0.2 | 130 | 25 | [52] |
| Banana stalk | FAS[1]/$H_2O_2$ | $Co^{2+}$ | 2.83 | 6.5 | 2.0 | 200 | 30 | [53] |
| Cellulose | Maleic anhydride | $Co^{2+}$ | 1.75[3] | 5.5 | 1.0 | - | 25 | [54] |
| Cellulose | Trimellitic anhydride | $Co^{2+}$ | 0.749 | 5.5 | 0.2 | 130 | 25 | (This study) |
| Cellulose | Succinic anhydride/mercerized | $Cu^{2+}$ | 2.421 | 5.4 | 1.0 | - | 25 | [55] |
| Sugar cane bagasse | Phthalic anhydride | $Cu^{2+}$ | 0.845 | 5.5 | 0.2 | 130 | 25 | [51] |
| Sugar cane bagasse | Trimellitic anhydride | $Cu^{2+}$ | 1.121 | 5.5 | 0.2 | 130 | 25 | [52] |
| Graphene oxide | $Fe_3O_4$ | $Cu^{2+}$ | 0.287 | 5.3 | 0.4 | - | 20 | [56] |
| Cellulose | Mercerized/EDTAD[2] | $Cu^{2+}$ | 1.050 | 5.3 | 1.0 | - | 25 | [57] |
| Cellulose | Trimellitic anhydride | $Cu^{2+}$ | 1.487 | 5.5 | 0.2 | 130 | 25 | (This study) |
| Sugar cane bagasse | Phthalic anhydride | $Ni^{2+}$ | 0.701 | 5.75 | 0.2 | 130 | 25 | [51] |
| Sugar cane bagasse | Trimellitic anhydride | $Ni^{2+}$ | 1.295 | 5.75 | 0.2 | 130 | 25 | [52] |
| Carbon nanotube | - | $Ni^{2+}$ | 0.949 | 5.0 | 0.2 | - | 27 | [58] |
| Graphene oxide | - | $Ni^{2+}$ | 1.75 | 5.0 | 0.4 | - | 27 | [59] |
| Carbon nanotube | Oxidation | $Ni^{2+}$ | 1.75 | 5.0 | 0.75 | - | 18 | [60] |
| Cellulose | Maleic anhydride | $Ni^{2+}$ | 2.40[3] | 5.5 | 1.0 | - | 25 | [54] |
| Cellulose | Trimellitic anhydride | $Ni^{2+}$ | 1.001 | 5.5 | 0.2 | 130 | 25 | (This study) |

[1] Ferrous ammonium sulfate; [2] EDTA dianhydride; [3] Obtained of modified Langmuir isotherm.

**Graphical abstract**